Plant Physiology®

Plant Physiology, 2025, 198, kiaf268
https://doi.org/10.1093/plphys/kiaf268
Advance access publication 24 June 2025
Research Article

A *trans*-long-chain prenyl diphosphate synthase promotes ubiquinone 10 biosynthesis in grape

Peipei Wang,[1,†] Tingting Ren,[1,2,†] Ruyue You,[1,2] Yazheng Cao,[3] Yang Xu,[3] Guo Wei,[3] Yuting Liu,[1] Xinglong Ji,[1,2] Yiran Ren,[1,2] Kekun Zhang,[4] Yongfeng Zhou,[5,6,*] Lei Sun,[7,*] Xiangpeng Leng[1,2,*]

[1]Institute of Grape Science and Engineering, College of Horticulture, Qingdao Agricultural University, Qingdao 266109, China
[2]Engineering Laboratory of Genetic Improvement of Horticultural Crops of Shandong Province, College of Horticulture, Qingdao Agricultural University, Qingdao 266109, China
[3]College of Horticulture and Landscape Architecture, Yangzhou University, Yangzhou 225009, China
[4]College of Enology, Northwest A&F University, Yangling 712100, China
[5]National Key Laboratory of Tropical Crop Breeding, Shenzhen Branch, Guangdong Laboratory of Lingnan Modern Agriculture, Key Laboratory of Synthetic Biology, Ministry of Agriculture and Rural Affairs, Agricultural Genomics Institute at Shenzhen, Chinese Academy of Agricultural Sciences, Shenzhen 518120, China
[6]National Key Laboratory of Tropical Crop Breeding, Tropical Crops Genetic Resources Institute, Chinese Academy of Tropical Agricultural Sciences, Haikou 571101, China
[7]Institute of Forestry and Pomology, Beijing Academy of Agriculture and Forestry Sciences, Beijing 100093, PR China
*Author for correspondence: zhouyongfeng@caas.cn (Y.Z.), sunlei@baafs.net.cn (L.S.), lengpeng2008@163.com (X.L.)
[†]These authors contributed equally to this work.
The author responsible for distribution of materials integral to the findings presented in this article in accordance with the policy described in the Instructions for Authors (https://academic.oup.com/plphys/pages/General-Instructions) is: Xiangpeng Leng (lengpeng2008@163.com); Lei Sun (sunlei@baafs.net.cn); Yongfeng Zhou (zhouyongfeng@caas.cn).

Abstract

Prenyl diphosphate synthase (PDS) plays indispensable roles in terpene biosynthesis. However, there is an ongoing debate regarding whether grape (*Vitis vinifera*) geranyl diphosphate synthase (VvGDS, VIT_15s0024g00850) can generate geranyl diphosphate (GPP), the precursor of monoterpene biosynthesis. Here, we demonstrated that VvGDS localizes in mitochondria and is an authentic *trans*-long-chain PDS (thus, VvGDS was renamed VvPDS), which is essential for ubiquinone (UQ) biosynthesis. This finding is in contrast to the initial association of VvPDS with GDS activity related to monoterpene biosynthesis. VvPDS not only falls within the subgroup comprising mitochondrial *trans*-long-chain PDSs, which participate in UQ biosynthesis in other eukaryotes, but also exhibits a positive association with UQ10 content in different grape tissues. VvPDS cannot catalyze GPP biosynthesis using isopentenyl diphosphate and dimethylallyl diphosphate as substrates. Furthermore, VvPDS functionally complements the yeast *coq1* mutation lacking mitochondrial hexaprenyl diphosphate synthase activity and catalyzes UQ10 and UQ9 biosynthesis. Transient overexpression of *VvPDS* in grape leaves increased UQ10 accumulation, whereas silencing *VvPDS* caused an obvious reduction in UQ10 content. Similarly, the stable overexpression of *VvPDS* enhanced UQ10 accumulation in tobacco (*Nicotiana tabacum*), and these UQ10-overproducing plants exhibited improved oxidative stress tolerance, primarily through enhanced reactive oxygen species-scavenging capacity. Taken together, these findings provide biochemical and genetic evidence supporting UQ biosynthesis in grape and encourage future research to reevaluate the enzymatic functions and physiological roles of angiosperm PDSs.

Introduction

Terpenes (also known as terpenoids) comprise the largest and structurally diverse class of natural products, with over 55,000 members have been identified in living organisms (Koksal et al. 2011; Vranová et al. 2012; Paramasivan and Mutturi 2017). In plant kingdom, terpenes play indispensable functions during plant growth and development, functioning as defense-related molecules (monoterpenes, sesquiterpenes, and diterpenes), photosynthetic pigments (chlorophylls and carotenoids), electron transporters (plastoquinones, PQs and ubiquinones, UQs), and phytohormones (abscisic acid, gibberellic acid, cytokinins, and brassinosteroids) (Aharoni et al. 2005; Gershenzon and Dudareva 2007; Tholl and Lee 2011; Moses et al. 2013; Tetali 2019). Despite their structural diversity and complexity, all terpenes originate from the common 5-carbon precursors, isopentenyl diphosphate (IPP), and its isomer dimethylallyl diphosphate (DMAPP), which are produced by the cytosolic mevalonic acid (MVA) pathway and the methylerythritol 4-phosphate pathway in plastids (Vranová et al. 2013). IPP and DMAPP are subsequently condensed to assemble prenyl diphosphates through a series of prenyl diphosphate synthases (PDSs), also called prenyltransferases (PTs) (Hsieh et al. 2011; Vranová et al. 2012).

The PDSs can be categorized into 2 structurally and evolutionarily different classifications, including either *cis*- or *trans*-PDSs, depending on the stereochemistry of the carbon-carbon double-bond in the products, and the enormous diversity of terpenes are originated from the products of *trans*-PDSs (t-PDSs) (Feng et al. 2020; Zhang et al. 2022). According to the chain length of main products, t-PDSs are further divided into short-chain (*trans*-SC-PDSs, C_{10} to C_{25}), medium-chain (*trans*-MC-PDSs, C_{30} to C_{35}), and long-chain (*trans*-LC-PDSs, C_{40} to C_{50}) PDSs (Vandermoten et al. 2009; Zhang et al. 2022; Wang et al. 2023b). Among the *trans*-SC-PDSs, geranyl diphosphate synthases (GDSs), farnesyl diphosphate synthase and geranylgeranyl diphosphate synthases (GGDSs) produce geranyl diphosphate (GPP) for C_{10} monoterpenes, farnesyl diphosphate (FPP) for C_{15}

Received January 3, 2025. Accepted March 14, 2025.

sesquiterpenes and geranylgeranyl diphosphate (GGPP) for C_{20} diterpenoids, respectively (Wang et al. 2016; Athanasakoglou et al. 2019). Specifically, GDS enzymes have been characterized in various plant species and exist as either homodimeric structures in both angiosperms and gymnosperms or heterodimeric structures in angiosperms (Burke et al. 1999; Burke and Croteau 2002; Tholl et al. 2004; Schmidt and Gershenzon 2008; Orlova et al. 2009; Rai et al. 2013; Chen et al. 2015; Yin et al. 2017). Heterodimeric GDSs consist of a non-catalytic small subunit (SSU) and a large subunit (LSU), where the LSU can either be inactive (Burke et al. 1999) or function independently as GGDS (Tholl et al. 2004; Wang and Dixon 2009). The interaction between the 2 subunits results in an active heterodimeric GDS (Nagegowda and Gupta 2020).

Among the *trans*-LC-PDSs, solanesyl diphosphate synthase (SDS) and decaprenyl diphosphate synthase (DDS) can further elongate the short chain prenyl diphosphate products (FPP and GGPP) to form solanesyl diphosphate (SPP, C_{45}) for PQ in plastids and decaprenyl diphosphate (C_{50}) for UQ in mitochondria, respectively (Jones et al. 2013; Liu and Lu 2016). PQs and UQs are 2 crucial prenylquinones, acting as electrons carriers in the oxygenic photosynthesis and aerobic respiratory electron transport chain, which located in chloroplast thylakoids and mitochondrial inner membrane, respectively (Swiezewska 2004; Parmar et al. 2015; Liu and Lu 2016; Fan et al. 2021). Both PQ and UQ are involved not only in plant stress responses as antioxidants, but also in the biosynthesis or catabolism of important chemical compounds (Liu and Lu 2016). The application of UQ, particularly UQ10, has widely used in people's health due to its crucial clinical benefits in Alzheimer's, Parkinson's and cardiovascular diseases (Kawamukai 2018). Interestingly, the length of the prenyl side chain and the type of UQs are highly variable in different species. For example, *Escherichia coli*, *Saccharomyces cerevisiae* and *Schizosaccharomyces pombe* produce UQ8, UQ6, and UQ10, respectively (Kawamukai 2002, 2009, 2018). Plants such as Arabidopsis and *Oryza sativa* synthesize UQ9 (Ohara et al. 2010; Ducluzeau et al. 2012), whereas most vegetables and fruits, including cauliflower, strawberry, orange, apple, and grape, mainly produce UQ10 (Mattila and Kumpulainen 2001; Teixeira et al. 2023).

Although UQs play essential roles in plants, *trans*-LC-PDSs involved in the biosynthesis of UQ side chains have only been functionally identified in Arabidopsis, *O. sativa*, tomato, and *Salvia miltiorrhiza* (Ohara et al. 2010; Ducluzeau et al. 2012; Jones et al. 2013; Liu et al. 2019a). For example, At2g34630 has been identified as a medium/long-chain PDS (AtPDS) located in mitochondria, which is responsible for UQ biosynthesis in *Arabidopsis* (Hsieh et al. 2011; Ducluzeau et al. 2012), rather than a homomeric GDS, a short-chain PDS required for monoterpenes biosynthesis, as originally proposed (Bouvier et al. 2000; Van Schie et al. 2007). Furthermore, rice *OsSDS1* and tomato *SlPDS* genes are responsible for the production of the prenyl side chain of UQ9 and UQ10, respectively (Ohara et al. 2010 ; Jones et al. 2013), whereas SmPDS catalyzes the formation of both UQ-9 and UQ-10 in *S. miltiorrhiza* (Liu et al. 2019a). Currently, other long-chain PDS genes involved in UQ side chain biosynthesis are still unknown in fruit crops, and comprehensive characterizations are indispensable to investigate the whole UQ biosynthetic pathway of plants.

Grape (*Vitis vinifera*) is 1 of the most widely cultivated and commonly consumed fruit crop with excellent nutritional value and unique aroma. Terpenes, particularly monoterpenes, are the most important and abundant class of volatile compounds, which are responsible for the flavor and aroma of Muscat grape (Leng et al. 2023; Shi et al. 2023). However, the functional characterization and enzyme activity analysis of both *trans*-SC- and *trans*-LC-PDSs remains largely unknown, with some perplexing discoveries also present in grape. For instance, gene expression and transcriptomic research indicated that the expression of *VvGDS* (VIT_15s0024g00850), a *trans*-SC-PDS as previously reported (Clastre et al. 1993), is positively associated with monoterpenes accumulation during berry ripening and potentially involved in the flux of monoterpene biosynthesis in grape (Martin et al. 2012; Ji et al. 2021; Wang et al. 2021; Yue et al. 2021a,b,c, 2022; Zhou et al. 2022; Xie et al. 2023). However, additional studies have shown no obvious associations between *VvGDS* gene expression and monoterpene accumulation (Sun et al. 2015; Wen et al. 2015; Liu et al. 2022; Leng et al. 2023). These findings raise our interest to reveal the authentic enzyme activity and function of GDS in grape. In this study, we conducted a comprehensive characterization of homodimeric VvGDS through both biochemical and genetic complementation analyses, and unveiled its involvement in UQ biosynthesis. Our results clearly demonstrated that VvGDS was localized within mitochondria and encoded an authentic *trans*-LC-PDS, which played an indispensable role in UQ10 biosynthesis in grape, rather than a GDS enzyme as previously reported (Clastre et al. 1993). Therefore, we renamed the homodimeric VvGDS to VvPDS (VIT_15s0024g00850) according to its enzyme activity. These findings provide better understanding of the *trans*-LC-PDS in grape and encourage us to reevaluate the enzyme activity and physiological functions of angiosperm GDSs.

Results

The expression of *VvPDS* showed a weak positive association with the monoterpene accumulation in grape

To elucidate the function of *VvPDS* in grape, we initially analyzed the association between *VvPDS* gene expression and monoterpene accumulation at 3 developmental stages of 4 grape cultivars, including 2 muscat-flavored grape cultivars ("Jumeigui" and "Muscat Hamburg") and 2 non-muscat aromatic cultivars ("Fujiminori" and "Kyoho"), due to the excellent nutritional and unique aroma originating from grape berries. Figure 1A illustrated that the total monoterpene contents in 2 muscat-flavored grape cultivars exhibited notable increases throughout berry development, rising by 5-folds from the green berries (EL34) to ripening (EL38) periods (Fig. 1A, Supplementary Table S1). However, the total monoterpene contents in 2 non-muscat aromatic cultivars exhibited only slight increases during the ripening phase, with "Fujiminori" and "Kyoho" showing increment of 1.8 to 2.2-folds, respectively, from green berries (EL34) to ripening (EL38) stage. Furthermore, reverse transcription quantitative PCR (RT-qPCR) analysis suggested that *VvPDS* shared similar gene expression patterns in all 4 grape cultivars, with a slight up-regulated during berry development and ripening (Fig. 1A). Meanwhile, a linear regression analysis revealed a coefficient of correlation of $R^2 = 0.4574$ (Fig. 1B), indicating a weak positive relationship between *VvPDS* gene expression and monoterpene accumulation in 4 grape cultivars. Although the accumulation of monoterpene data from this study do not reflect the natural emission of monoterpene in intact organs, which is limited for the dissection of functions of grape *VvPDS*, the integration of monoterpene profiling, RT-qPCR data and enzyme activity assay is a feasible strategy for validating the function of *VvPDS* at the molecular level as previously reported by Wei et al. (2016).

Additionally, methyl jasmonate (MeJA), a known monoterpene elicitor (De Geyter et al. 2012; D'Onofrio et al. 2018; Li et al. 2020), was used to further assess the association between *VvPDS* gene expression and monoterpene accumulation. In "Muscat Hamburg" grape, *VvPDS* exhibited an increased expression at

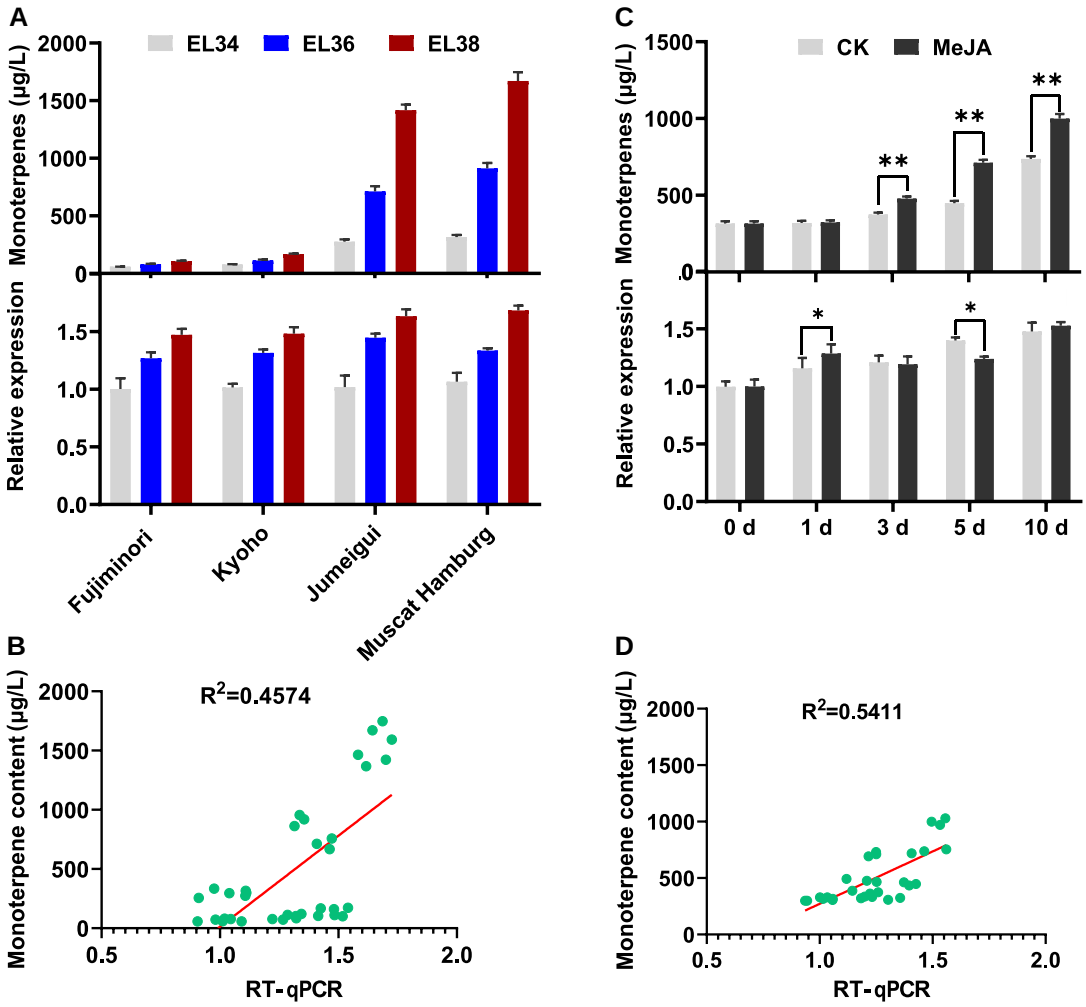

Figure 1. The correlation analysis between *VvPDS* gene expression and monoterpene content in grape. **A)** *VvPDS* gene expression and monoterpenes content in 4 grape cultivars, including "Fujiminori," "Kyoho," "Jumeigui" and "Muscat Hamburg." **B)** Correlation of monoterpenes content (*y* axis) and *VvPDS* gene expression (*x* axis) in 4 grape cultivars. **C)** *VvPDS* gene expression and monoterpenes content in response to MeJA treatment in "Muscat Hamburg" grape. **D)** Correlation of monoterpenes content (*y* axis) and *VvPDS* gene expression (*x* axis) in response to MeJA treatment. Data in **A)** and **C)** were means ± SD of 3 biological replicates. VvActin (AB073011) was used as the reference for **A)** and **C)**. Asterisks in **C)** indicated significant differences as determined by Student's *t*-test (*$P < 0.05$; **$P < 0.01$).

the first day in response to MeJA treatment. However, monoterpene accumulation obviously increased from the 3rd to 10th days after MeJA treatment (Fig. 1C, Supplementary Table S2). Furthermore, the correlation coefficient was only 0.5411 between *VvPDS* gene expression and monoterpene accumulation in response to MeJA (Fig. 1D). Taken together, the expression of *VvPDS* was found to be weakly positively associated with the monoterpene accumulation in grape.

VvPDS was evolutionarily more closely related to the *trans*-LC-PDSs

The multiple sequence alignment revealed that VvPDS, along with other plant *trans*-LC-PDSs proteins, contained the typical conserved domains of PDSs from various plants (Supplementary Fig. S1, Hsieh et al. 2011; Liu et al. 2019b). VvPDS encoded a protein consisting of 422 amino acids and possessed 2 conserved aspartate-rich motifs ($DDx_{2\text{-}4}D$ and DDxxD) (Supplementary Fig. S1), which are widely recognized in many PDSs and are responsible for binding prenyl diphosphate substrates (Wang and Ohnuma 1999; Wang et al. 2016).

Through sequence identity and analysis, it was observed that VvPDS exhibited high similarity (more than 65%) with other known *trans*-LC-PDSs found in various angiosperm plants (Supplementary Fig. S2). These proteins are generally localized in the mitochondria, produce compounds with more than C_{35} carbon atoms, and are involved in UQ biosynthesis (Ohara et al. 2010; Hsieh et al. 2011; Jones et al. 2013; Liu et al. 2019b). VvPDS exhibited 30% to 35% similarity with known solanesyl diphosphate synthases (SPS) (Supplementary Fig. S2), which are localized in the chloroplasts and contribute to PQ biosynthesis (Ohara et al. 2010; Jones et al. 2013; Liu et al. 2019b). Conversely, VvPDS showed the lower similarity with heteromeric GGDS/GDS (<30%; Supplementary Fig. S2), which are involved in monoterpene biosynthesis in various plants (Tholl et al. 2004 ; Chen et al. 2015; Wei et al. 2016). These results suggest that VvPDS may perform analogous functions with *trans*-LC-PDSs.

Furthermore, the phylogenetic analysis revealed that VvPDS exhibited more closer relationship with other *trans*-LC-PDSs than with *trans*-SC-PDSs (e.g. GDS and GGDS) (Fig. 2A). *trans*-LC-PDSs were further classified into 2 independent subfamilies: the mitochondrial or plastidial ones (Fig. 2A). VvPDS was assigned a member of the

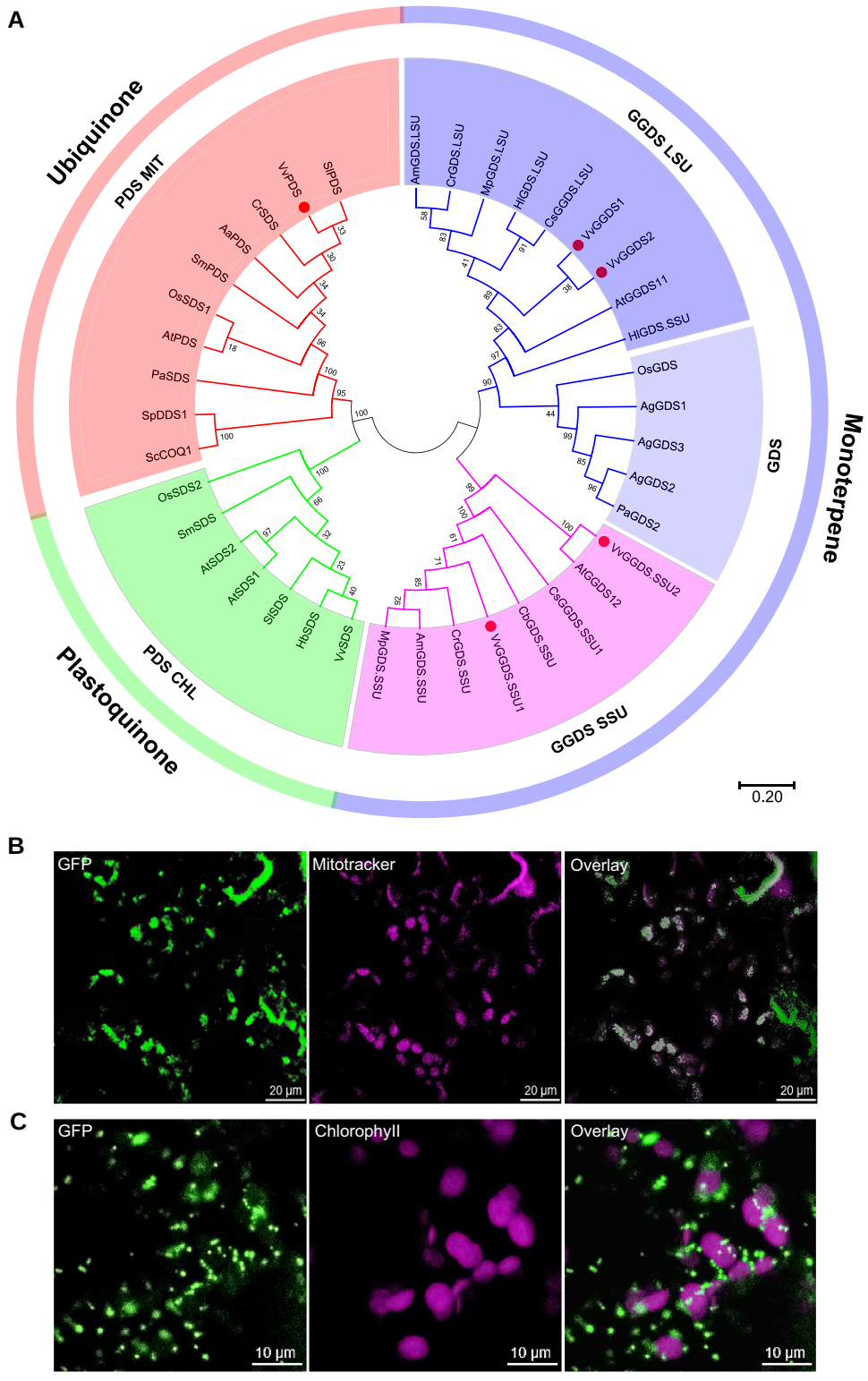

Figure 2. Subcellular localization of VvPDS and phylogenetic analysis of plant PTs. **A)** The phylogenetic tree was constructed by MEGA7 with the neighbor-joining test and 1,000 bootstrap replicates. MIT, mitochondria; CHL, chloroplast. **B)** and **C)** Transient expression of VvPDS-GFP in *N. benthamiana* leaves. GFP, green fluorescent protein; Mitotracker, purple pseudocolor of Mitotracker; Chlorophyll, purple pseudocolor of plastid autofluorescence; Overlay, the merged image.

mitochondrial subfamily, which included other known *trans*-LC-PDSs involved in the UQ biosynthesis, such as OsSDS1, AtPDS, SlPDS, SmPDS, and yeast COQ1 (hexaprenyl diphosphate synthase; Fig. 2A; Ohara et al. 2010; Ducluzeau et al. 2012; Jones et al. 2013; Liu et al. 2019b). Accordingly, VvPDS was predicted to contain mitochondrial and chloroplast signal peptide sequence based on the protein localization programs, TargetP and WoLF PSORT. To validate the subcellular localization, the full length VvPDS was fused with a green fluorescent protein (GFP) gene and transiently transformed into *Nicotiana benthamiana* leaves. Transient expression of

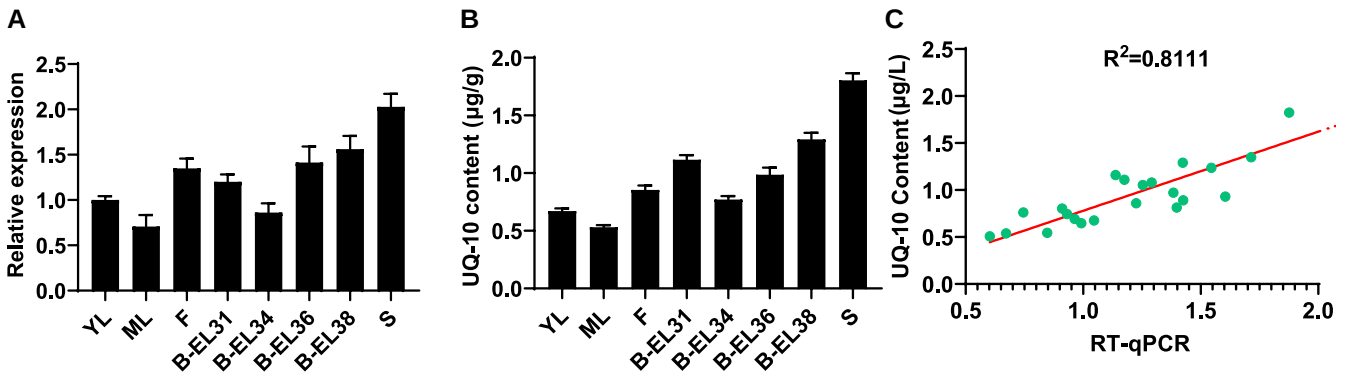

Figure 3. The correlation analysis between *VvPDS* gene expression and UQ content in grape. **A)** The tissue-specific expression profile of *VvPDS* in young leaf (YL), mature leaf (ML), flowers (F), berries pea-size (B-EL31), berries begin to soften (B-EL34), berries with intermediate Brix values (B-EL36), Berries harvest-ripe (B-EL38), and developing seeds at veraison (S). Data were means ± SD of 3 biological replicates. VvActin (AB073011) was used as the reference. **B)** UQ10 content in different tissues of grape by HPLC analysis. Data were means ± SD of 3 biological replicates. **C)** Correlation of UQ10 content (*y* axis) and *VvPDS* gene expression (*x* axis) in different tissues of grape.

the VvPDS-GFP in *N. benthamiana* leaf tissues resulted in a punctate pattern of green fluorescence, which clearly co-localized with the mitochondrial red fluorescent protein marker (Fig. 2B), whilst no GFP overlap could be found with the autofluorescence of chloroplasts (Fig. 2C). There results indicated that VvPDS was exclusively located in mitochondria and not present in chloroplasts.

VvPDS was positively associated with the UQ10 accumulation in grape

Previously published transcriptomic databases (Fasoli et al. 2012) showed that *VvPDS* exhibited widespread expression in nearly all tissues, with slightly higher expression in developing seeds during véraison and mid-ripening compared with pollen, mature tendrils, and carpel (Supplementary Fig. S3 and Table S3). We further confirmed that *VvPDS* displayed the highest expression in seeds, followed by mature berries, while its expression is relatively low in mature leaves, as determined by RT-qPCR (Fig. 3A). Furthermore, detection by LC-MS/MS demonstrated that the major UQ component (UQ10) was widely distributed throughout the various tissue of grape with highest level in seeds and lowest level in mature leaves (Fig. 3B, Supplementary Fig. S4). Furthermore, the expression level of *VvPDS* exhibited positive association with UQ10 content and the correlation coefficient reached 0.8111 (Fig. 3C), aligning with the predicted role of *VvPDS* in UQ10 biosynthesis. Notably, we did not detect UQ9 in various grape tissue (Supplementary Fig. S4), which may be due to the relatively low content of UQ9 in grape. Previous studies also showed that UQ10 was main UQ components in grape, which showed higher content than UQ9 in different tissue (Teixeira et al. 2020, 2023).

VvPDS lacks GPP synthesis ability but complements yeast *coq1* knockout

We proceeded to investigate whether VvPDS is capable of synthesizing GPP, the enzyme activity in vitro was conducted by utilizing DMAPP and IPP as substrates. Gas chromatograph-mass spectrometer (GC-MS) results demonstrated that VvPDS protein lacked the capacity to synthesize GPP (Fig. 4A). Similarly, the *trans*-LC-PDS, AtPDS, also lacked GPP synthesis ability, whereas the known *trans*-SC-PDS, OsGDS (Zhou et al. 2017), exhibited the ability to synthesize GPP (Fig. 4A). Taken together, our results indicated that VvPDS is not a GPP synthase.

Phylogenetic analyses, subcellular localization and expression pattern data led us to speculate that *VvPDS* was an authentic *trans*-LC-PDS gene that specifically produced the side chain of UQ in grape. To verify this hypothesis, the full-length cDNA of *VvPDS* was inserted into the yeast D-galactose inducible expression vector pRS426, and this recombinant construct was introduced into a *S. cerevisiae coq1* knockout strain (3138). The *coq1* mutant, lacking mitochondrial hexaprenyl diphosphate synthase activity, cannot produce UQ and consequently is unable to grow on non-fermentable carbon substrates (Ashby and Edwards 1990; Ducluzeau et al. 2012). The expression of *VvPDS* successfully reinstated the mutant cells' ability to utilize glycerol and ethanol as carbon sources, a function consistent with that of AtPDS, serving as a positive control. In contrast, no functional complementation was found when the mutant cells were transformed with empty vector and OsGDS (Fig. 4B), which is a *trans*-SC-PDS and produce GPP for C_{10} monoterpenes (Zhou et al. 2017).

LC-MS/MS analysis displayed that strain 3138 expressing AtPDS generated UQ9, while cells harboring the VvPDS construct produced UQ10 along with a small amount of UQ9 (Fig. 4C). In contrast, no UQ was detected in strain 3138 with the empty vector pRS426 or OsGDS (Fig. 4C). Additionally, the UQ9 content in these 2 complemented strains was nearly identical, and the strains hosting the VvPDS construct produced more UQ10 than UQ9 (Fig. 4D). Taken together, these findings clearly indicated that VvPDS was a genuine *trans*-LC-PDS, actively contributing to UQ10 and UQ9 biosynthesis in grape.

Altered expression of *VvPDS* influences the accumulation of UQ10

To further ascertain the function of *VvPDS* in grape, stable expression assays were carried out in *Nicotiana tabacum* through *Agrobacterium*-mediated transformation. Three representative *VvPDS*-OE lines (T3) were selected for further study after confirmation of high *VvPDS* transcript levels using RT-qPCR analysis (Fig. 5A). Corresponding with these expression patterns, LC-MS/MS analysis showed that the UQ10 content in 3 transgenic lines increased by 1.5 to 2.0-fold compared with wild type (WT) plants (Fig. 5, B and E). Interestingly, *NtSDS* (LOC107776134), the homolog of *VvPDS*, showed down-regulated expression in 3 transgenic lines compared with WT (Supplementary Fig. S5D), indicating the UQ products may cause feedback inhibition of UQ biosynthesis. To eliminate the controversial function of *VvPDS* in monoterpene biosynthesis, we also measured the monoterpene accumulation in *VvPDS* transgenic plants. Our observations indicated that 3 *VvPDS*-OE

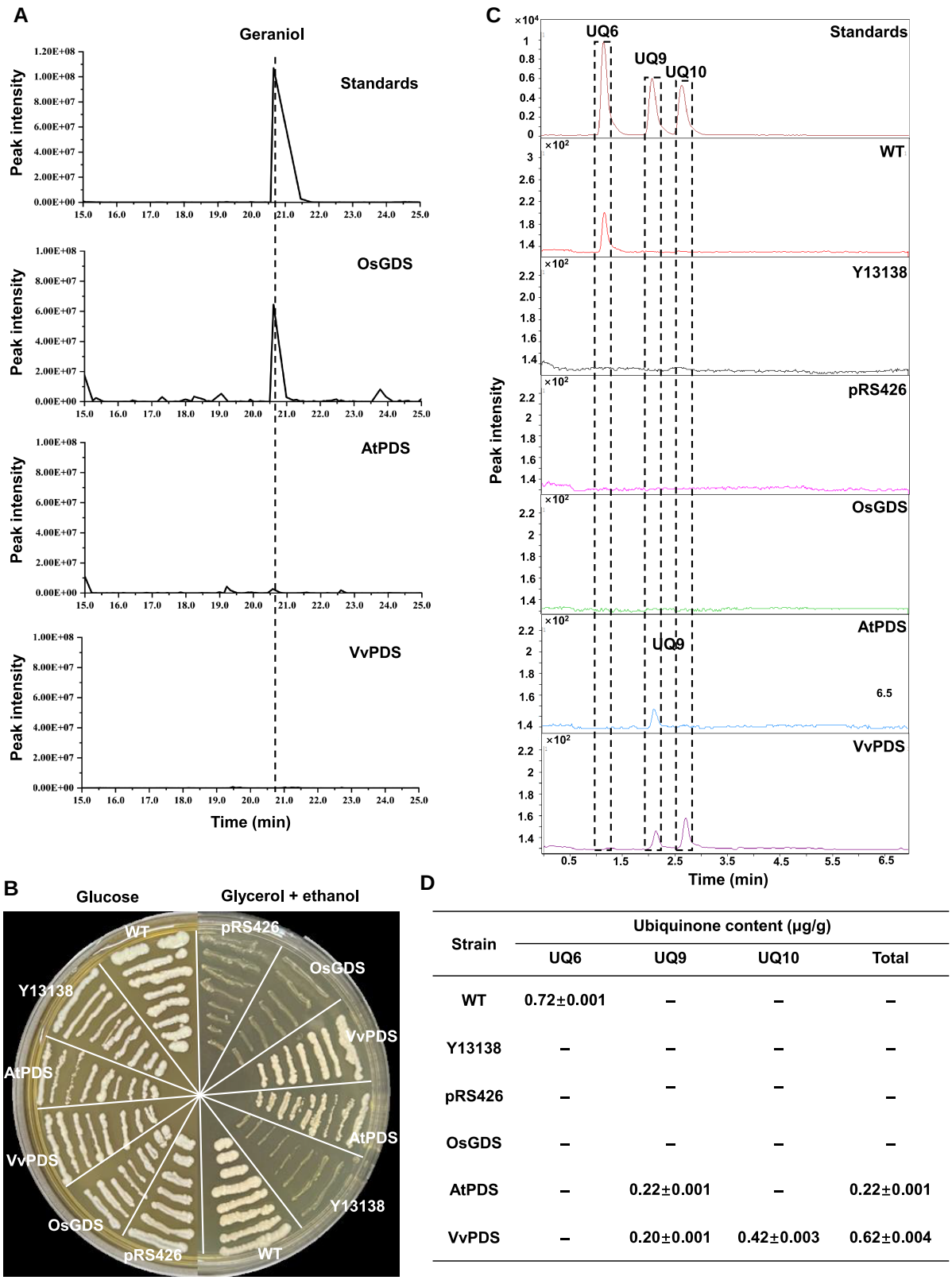

D

Strain	Ubiquinone content (μg/g)			
	UQ6	UQ9	UQ10	Total
WT	0.72±0.001	–	–	–
Y13138	–	–	–	–
pRS426	–	–	–	–
OsGDS	–	–	–	–
AtPDS	–	0.22±0.001	–	0.22±0.001
VvPDS	–	0.20±0.001	0.42±0.003	0.62±0.004

Figure 4. Enzyme activity assay for functional characterization of VvPDS. **A)** GC-MS chromatograms showed the products generated by VvPDS from isopentenyl pyrophosphate (IPP) and DMAPP as substrates in vitro. OsGDS (Os01g14630) and AtPDS (At2g34630) protein were used as positive and negative control, respectively. **B)** VvPDS functionally complemented the yeast coq1 knockout mutant. Wild-type (WT) and *coq1* mutant yeast harboring empty vector (pRS426), OsGDS, AtPDS or VvPDS cDNAs were plated on an YPD medium with glucose as the carbon source, or an YPEG medium with glycerol and ethanol (non-fermentable) as the carbon sources and 0.05% D-galactose as the inducer. Plates were incubated at 30 °C for 2 d (glucose) or 7 d (glycerol/ethanol). **C)** and **D)** LC-MS/MS chromatograms showing the UQ products **C)** and contents **D)** in WT yeast and yeast coq1 knockout strain 3138 harboring empty vector (pRS426), OsGDS, AtPDS or VvPDS, respectively. Dashes indicated that no UQ was detected. Data were means ± SD of 3 replicates in **D)**.

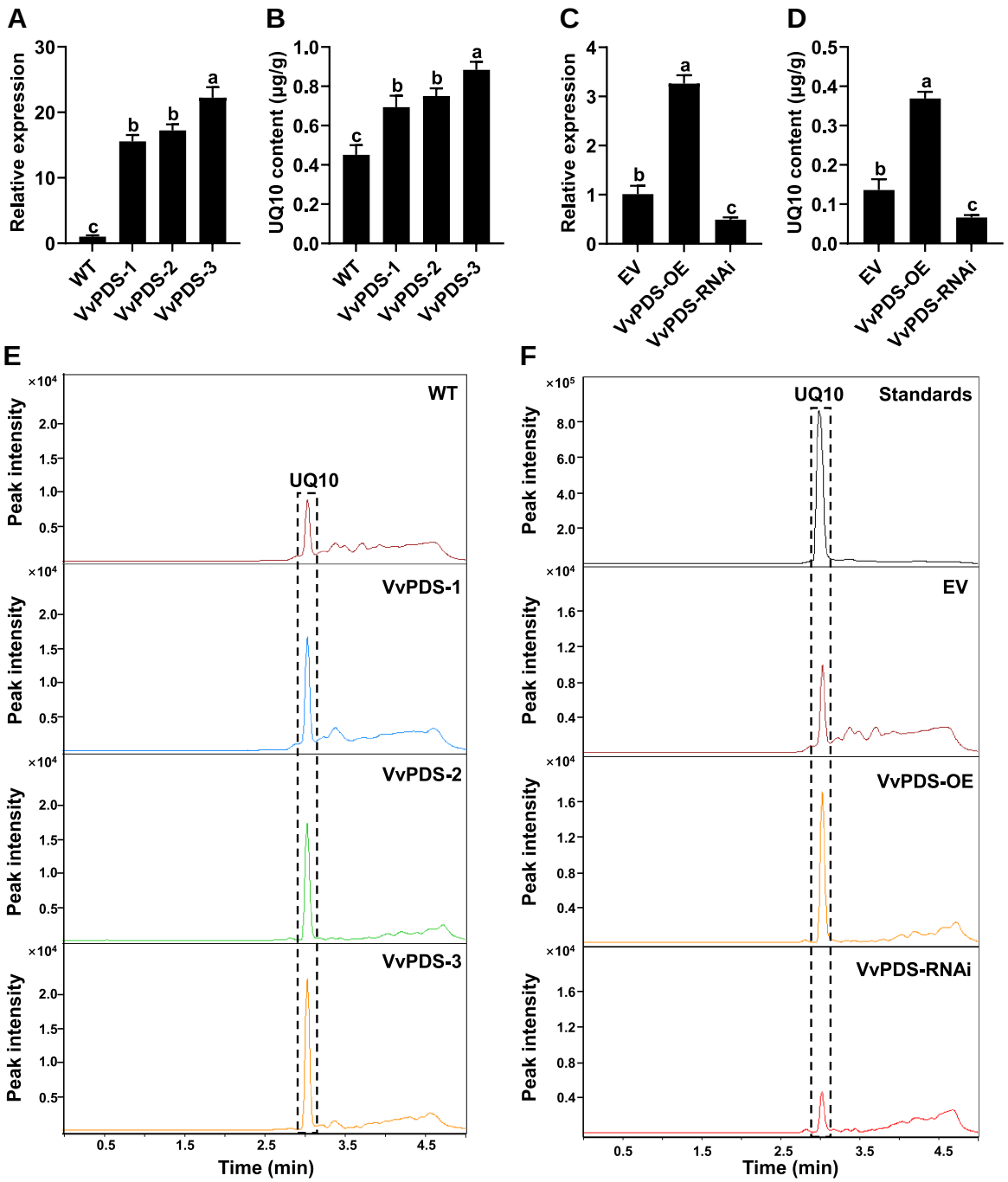

Figure 5. Stable and transient transformation of VvPDS in tobacco and grape. **A)** RT-qPCR analysis of VvPDS mRNA levels in WT and transgenic tobacco plants by stable overexpression. *NtActin* (GQ281246) was used as the reference. **B)** UQ10 content in WT and transgenic tobacco plants by stable overexpression. **C)** RT-qPCR analysis of VvPDS mRNA levels in VvPDS-overexpression, RNAi, and WT grape leaves. *VvActin* (AB073011) was used as the reference. **D)** UQ10 content in VvPDS-overexpression, RNAi, and WT grape leaves; **E)** and **F)** LC-MS/MS analysis of UQ10 products in tobacco **E)** and grape **F)**, respectively. Data were means ± SD of 3 biological replicates and different letters indicated significant differences ($P < 0.05$) based on Duncan's test in **A)** to **D)**.

lines did not alter the monoterpenes accumulation when compared with WT plants (Supplementary Fig. S5, A to C), which was consistent with our previous results that *VvPDS* lacked GPP synthesis ability and is unable to generate GPP for monoterpene biosynthesis (Fig. 4A).

To validate the involvement of *VvPDS* in UQ10 biosynthesis in grape, a transient transformation system was performed in the leaves of Chinese wild grapevine species *Vitis quinquangularis* accession "Danfeng-2," which have been widely used for gene function validation by the transient transformation method in grape (Wang and Wang 2019; Liu et al. 2022; Wei et al. 2023). The transient overexpression of *VvPDS* in wild grapevine leaves obviously induced UQ10 accumulation after 3 d of transformation compared with the control leaves. Conversely, UQ10 accumulation was obviously suppressed after silencing *VvPDS* in wild grapevine leaves (Fig. 5, D and F). RT-qPCR analysis further demonstrated that the expression level of *VvPDS* was up-regulated and down-regulated in the OE and RNAi leaves compared with the control

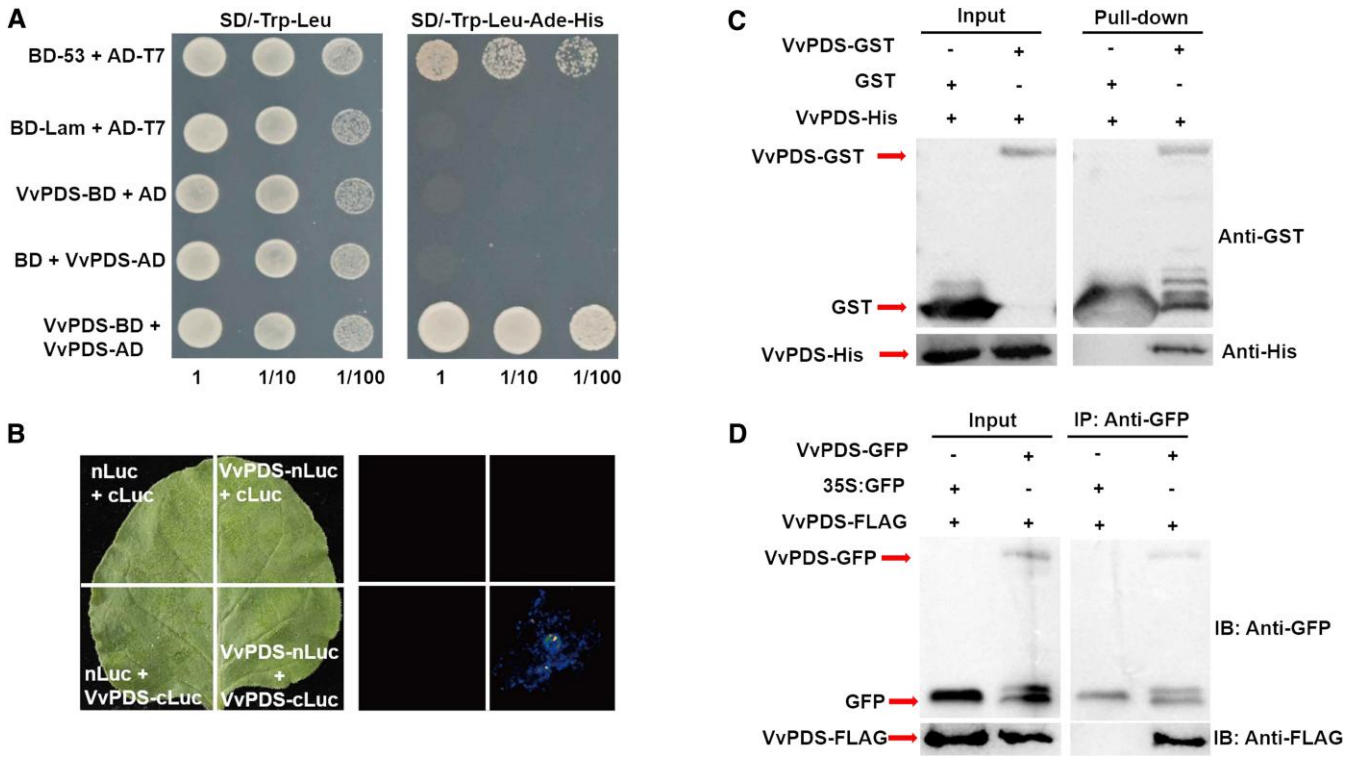

Figure 6. The homodimeric structure of VvPDS. **A)** The interaction between VvPDSs was analyzed by using an Y2H assay. BD-53 + AD-T7 and BD-Lam + AD-T7 were used as positive and negative controls, respectively. Transformed yeast cells were grown on SD/-Trp-Leu and SD/-Trp-Leu-Ade-His medium, respectively. **B)** Firefly LUC complementation imaging assay between VvPDSs in *N. benthamiana* leaves. **C)** In vitro pull-down analysis of VvPDS-VvPDS homodimeric interaction. Glutathione-S-transferase (GST)-VvPDS or GST proteins were incubated with VvPDS-His proteins, together with glutathione-sepharose beads in tubes. Bead-bound proteins were subjected to 12% (w/v) sodium dodecyl sulphate-polyacrylamide gel electrophoresis (SDS-PAGE); precipitated protein was detected using anti-His antibody. **D)** In vivo co-IP analysis of VvPDS-VvPDS homodimeric interaction in *N. benthamiana*. VvPDS-FLAG were co-expressed with VvPDS-GFP or GFP in *N. benthamiana* and subjected to anti-FLAG IP. Proteins were then subjected to anti-FLAG and anti-GFP immunoblotting.

(Fig. 5C). All these results collectively demonstrated that *VvPDS* positively regulated UQ10 accumulation in grape.

VvPDS belongs to the homodimeric PT family

PT in plant has been functionally characterized as homomeric and heteromeric enzymes (Rai et al. 2013; Chen et al. 2015). Therefore, we initially conducted yeast 2-hybrid (Y2H) assays to assess their homomeric architecture. Yeast cells carrying both VvPDS-pGBD and VvPDS-pGAD exhibited normal growth in selective medium (-Trp/-Leu/-His/-Ade), suggesting that VvPDS can form homodimers in yeasts (Fig. 6A). Subsequently, the homomeric interaction was further confirmed by luciferase (LUC) complementation experiment in vivo. The outcome clearly demonstrated co-transformation of VvPDS-nLUC and VvPDS-cLUC showed a strong LUC signal in *N. benthamiana* leaves (Fig. 6B). By contrast, LUC activity was barely detectable when leaves were infiltrated with other combinations (Fig. 6B). Moreover, these interaction results were further confirmed by GST pull-down and co-immunoprecipitation (co-IP) in vitro and vivo, respectively. The pull-down assay showed that VvPDS-His protein were enriched by VvPDS-GST, but not by GST alone (Fig. 6C), indicating the homomeric interaction of VvPDS in vitro. Finally, the co-IP assay exhibited that VvPDS protein was immunoprecipitated by the anti-GFP antibody in *N. benthamiana* leaves expressing VvPDS-FLAG, but not in the corresponding controls (Fig. 6D). All these results collectively supported the conclusion that VvPDS could form homodimers in grape. Similarly, AtPDS protein with homology to VvPDS was also designated as homomeric complex (Hsieh et al. 2011), indicating the proteins in this clade (Fig. 2A) were closer related to *trans*-LC-PDSs activity.

Additionally, 4 identified *trans*-SC-PDSs, including VvGGDS1 (VIT_04s0023g01210), VvGGDS2 (VIT_18s0001g12000), VvGGDS.SSU1 (VIT_19s0090g00530) and VvGGDS.SSU2 (VIT_03s0038g03050), were homologous to VvPDS, the *trans*-LC-PDS in the grape genome (Leng et al. 2023). The formation of heteromeric complex was also investigated between VvPDS and its homologous proteins. Y2H assays clearly demonstrated that there were no interactions between VvPDS and VvGGDS1, VvGGDS2, VvGGDS.SSU1, or VvGGDS.SSU2 (Supplementary Fig. S6). Combining data in phylogenetic analysis and subcellular localization, *trans*-SC and LC-PDS in grape were perfectly separated in 2 different groups, which might explain the absent of protein-protein interactions between *trans*-SC and LC-PDSs in grape. These results showed that *trans*-SC and LC-PDSs in grape might produce different chain of prenyl diphosphates and play different roles in various terpene biosynthesis pathways via homomeric or heteromeric proteins.

Overexpression of *VvPDS* increases oxidative stress tolerance

In comparison to WT tobacco (*N. tabacum*), UQ10-overproducing tobacco plants were expected to display enhanced resistance to oxidative stress since UQ10 can act as a potent antioxidant in plant cells (Wang and Hekimi 2016). To assess their response to oxidative stress, these transgenic and WT plants were subjected to 50 μM methyl viologen (MV), a powerful superoxide radical inducer. After 3 d of treatment, leaves of WT plants demonstrated more

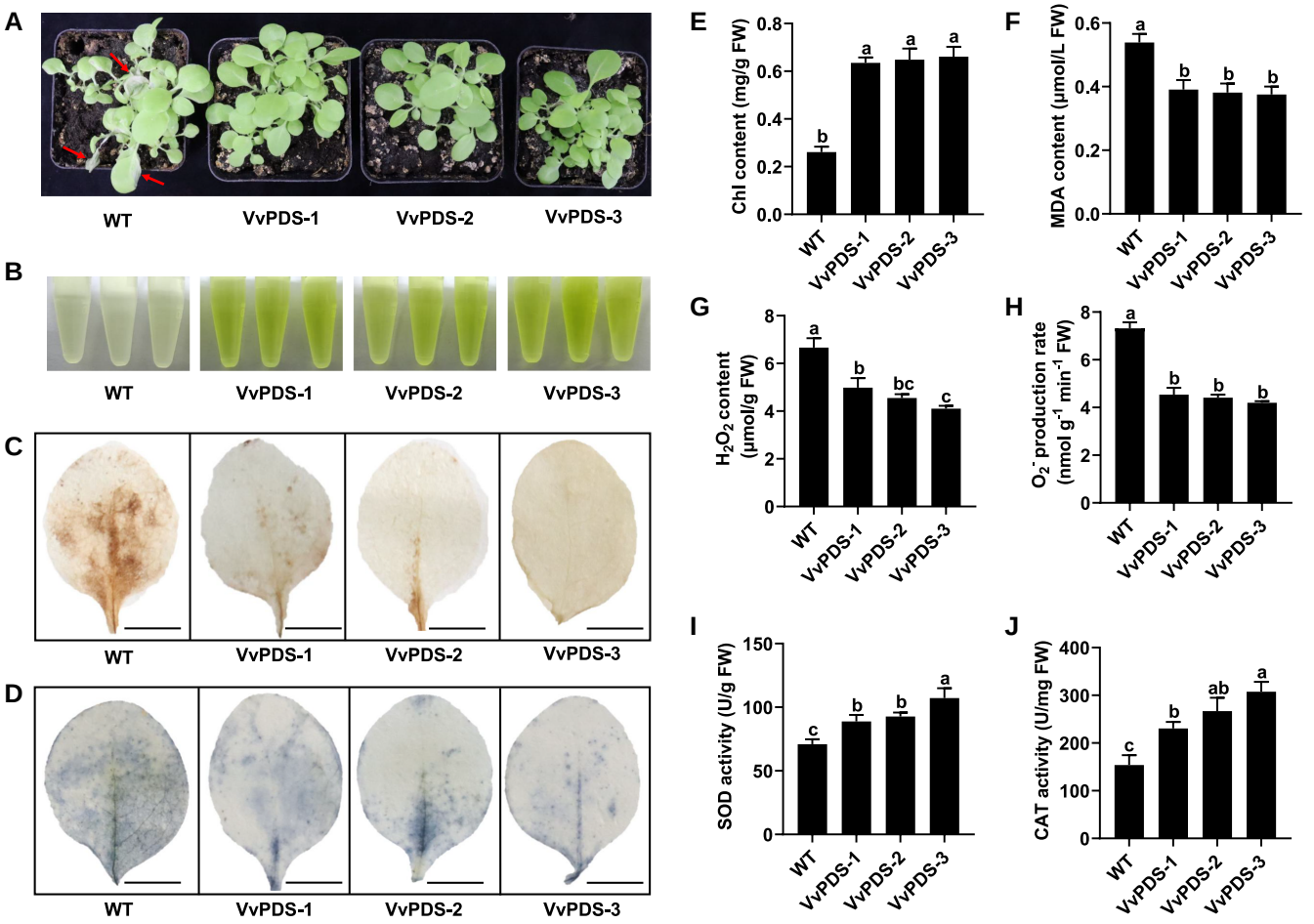

Figure 7. UQ10-overproducing tobacco increases MV stress tolerance and ROS-scavenging capacities. **A)** The phenotype between transgenic and WT tobacco leaves by MV treatment. **B)** and **E)** Chlorophyll (Chl) extraction solutions and Chl content in leaves of WT and VvPDS transgenic tobaccos. FW, fresh weight. **C)** and **G)** DAB staining and H_2O_2 contents of leaves in WT and VvPDS transgenic tobaccos after MV treatment, respectively. The scale bars represented 1.0 cm. **D)** and **H)** NBT staining and O_2^- contents of leaves in WT and VvPDS transgenic tobaccos after MV treatment, respectively. The scale bars represented 1.0 cm. **F)** MDA contents in WT and VvPDS transgenic tobaccos after MV treatment. **F)** SOD and CAT activity in WT and VvPDS transgenic tobaccos after MV treatment, respectively. Data were means ± SD of 3 biological replicates and different letters indicated significant differences ($P < 0.05$) based on Duncan's test in **E)** to **J)**.

severe visible injury compared with the UQ10-overproducing plants (Fig. 7A). The chlorophyll (Chl) content in the transgenic lines was obviously higher than in the WT plants (Fig. 7, B and E), confirming that the damage to chloroplast was lower in UQ10-overproducing plants under MV stress.

Meanwhile, the *VvPDS* transgenic lines exhibited a lower level of malondialdehyde (MDA) production compared with WT plants under MV-induced stress (Fig. 7F). Furthermore, the VvPDS-OE lines exhibited lighter brown or blue staining of the leaf when subjected to diaminobenzidine (DAB) and *p*-nitroblue tetrazolium chloride (NBT) treatment, denoting lower H_2O_2 or O_2^- accumulation than WT plants, respectively (Fig. 7, C and D). These observations were in line with the visible phenotype, as the VvPDS-OE plants exhibited lower level of H_2O_2 and O_2^- accumulation than WT plants under MV treatment (Fig. 7, G and H), implying that UQ10-overproducing plants might be closely related to the decrease of reactive oxygen species (ROS) accumulation. Additionally, the activities of superoxide dismutase (SOD) and catalase (CAT) were distinctly higher in *VvPDS* transgenic lines compared with WT plants under MV-induced stress (Fig. 7, I and J), suggesting that UQ10-overproducing plants achieved a reduction in oxidative damage by enhancing their ROS-scavenging abilities.

Discussion

Grape is 1 of the most important horticultural crops with excellent nutritional and unique aroma. Muscat grape cultivars are extensively popular for fresh consumption due to its pleasant rose-scented, which mainly depend on volatile terpenes, particularly monoterpenes (Liu et al. 2022; Bosman and Lashbrooke 2023; Leng et al. 2023). PDSs are important branching points in terpene biosynthesis, and largely determine the terpene diversity by dictating the prenyl chain elongation of prenyl diphosphates, such as GPP, FPP, and GGPP (Nagel et al. 2014). The production of GPP was acting as the precursor for the biosynthesis of volatile monoterpene, which not only makes important contributions to fruity and flowery notes, but also protects plants against diverse abiotic and biotic stresses (Pichersky et al. 2006; Rosenkranz et al. 2021; Leng et al. 2023). However, only scattered and unsystematic information is available about the function of PDSs in grape. Here, our findings unequivocally demonstrated that VvPDS encoded an authentic *trans*-LC-PDS and was responsible for UQ10 biosynthesis, rather than a GDS activity linked to monoterpene biosynthesis as previously proposed (Clastre et al. 1993; van Schie et al. 2007).

It is universally accepted that GPP and its downstream monoterpene are synthesized in plastids (Nagegowda 2010; Gutensohn et al.

2013; Dong et al. 2016; Nagegowda and Gupta 2020). However, subcellular localization analysis depicted that VvPDS was exclusively localized in mitochondria rather than in the chloroplasts (Fig. 2B), indicating VvPDS might lack monoterpene synthesis ability due to the difference in subcellular compartments between mitochondria and chloroplasts (Fig. 2A). This speculation was further confirmed by our enzyme activity analysis that VvPDS protein lacked the capacity to synthesize GPP by utilizing DMAPP and IPP as substrates (Fig. 4A), which was consistent with the previous result that AtPDS, a *trans*-LC-PDSs, cannot catalyze the synthesis of GPP from IPP and DMAPP (Hsieh et al. 2011). Similarly, our phylogenetic analysis also clearly demonstrated that VvPDS shares higher similarity with known mitochondria *trans*-LC-PDSs involved in UQ biosynthesis (Ohara et al. 2010; Hsieh et al. 2011; Jones et al. 2013; Liu et al. 2019b) than with chloroplast *trans*-SC-PDSs involved in monoterpene biosynthesis (Tholl et al. 2004; Chen et al. 2015; Wei et al. 2016; Fig. 2A; Supplementary Fig. S2).

Furthermore, *trans*-LC-PDSs were classified into 2 independent subclades: the mitochondrial or plastidial ones (Fig. 2A), which play important roles in UQ and PQ biosynthesis, respectively. For example, both AtSDS1 and AtSDS2 are exclusively located in plastids and responsible for the biosynthesis of PQ9 (Block et al. 2013). OsSDS2 and SlSDS are also targeted to the plastid and contribute to PQ9 production (Ohara et al. 2010; Jones et al. 2013). However, the mitochondria localization of VvPDS aligned with the previous findings regarding OsSDS1 (Ohara et al. 2010), AtPDS (Ducluzeau et al. 2012), SlPDS (Jones et al. 2013), and SmPDS (Liu et al. 2019b), suggesting that VvPDS might be involved in biosynthesis of the side chain of UQ. For example, AtPDS, OsSDS1 and SmPDS have demonstrated the ability to complement the yeast *coq1* mutant, in which the homodimeric-type hexaprenyl diphosphate synthase gene (COQ1) responsible for UQ biosynthesis is disrupted. Overexpression of *AtPDS*, *OsSDS1* and *SmPDS* led to obvious increase in UQ9 content, whereas down-regulation of *AtPDS* and *SmPDS* resulted in decreased UQ9 accumulation in transgenic plants (Ohara et al. 2010; Ducluzeau et al. 2012; Liu et al. 2019b). In this study, we found that VvPDS could complement UQ production in the *S. cerevisiae coq1* mutant, resulting in production of both UQ10 and UQ9 in yeast cells, with the major product being UQ10 (Fig. 4B). Functional analysis of *VvPDS* through stable overexpression in *N. tabacum* showed that *VvPDS* played a role in the biosynthesis of UQ10 (Fig. 5, A, B and E). Overexpression and silencing of *VvPDS* in wild grapevine leaves displayed increased and decreased UQ10 accumulation, respectively (Fig. 5, C, D and F). These results clearly showed that VvPDS possessed a *trans*-LC-PDS activity and contributed positively to UQ biosynthesis, refuting the former assumption of it being a homomeric C_{10}-GDS. Furthermore, *trans*-LC-PDSs responsible for synthesizing the side-chains of UQ are typically believed to be homodimeric enzymes (Kainou et al. 2001; Kawamukai 2002; Guo et al. 2004; Hsieh et al. 2011). For example, octaprenyl-diphosphate synthase (IspB), which is essential for the synthesis of the side chain of UQ8 in *E. coli*, forms a homodimer that is crucial for determining isoprenoid chain length (Kainou et al. 2001). However, in some cases, such as decaprenyl diphosphate synthase (Dds1) and its partner Dlp1, they form a heterotetrameric complex in Fission yeast (*S. pombe*) and together constitute the UQ10 enzymatic activity in *E. coli* (Saiki et al. 2003). Our findings demonstrated that VvPDS proteins could form homodimers but not heteromeric complex in grape through Y2H, LUC assays, pull-down and co-IP (Fig. 6; Supplementary Fig. S6), which was consistent with previous observations that AtPDS formed a stable homodimer under physiological conditions in *Arabidopsis* (Hsieh et al. 2011). Our findings not only reevaluate the originally reported homomeric VvGDS to be long-chain VvPDS but also reveal the actual role of homomeric VvPDS in the UQ10 (C_{50}) biosynthesis.

As a potent antioxidant or a signal regulating gene expression, UQ is directly or indirectly involved in plant stress resistance (Ohara et al. 2004; Dutta et al. 2015; Liu et al. 2019a). Overexpression of yeast *COQ2* in *N. tabacum* enhanced UQ10 content and elevated plant resistance to oxidative stresses induced by high salinity and MV (Ohara et al. 2004). In Arabidopsis, the UQ redox state mediated ROS levels and played a pivotal role in regulating the plant fundamental resistance against bacterial pathogens and high oxidative stress environments (Dutta et al. 2015). Our genetic transformation analysis showed that overexpression of VvPDS obviously increased UQ10 accumulation (Fig. 5). Although UQ10-overproduction *N. tabacum* plants did not show any morphological differences, these transgenic plants displayed enhanced oxidative stress tolerance along with higher SOD and CAT activities and lower H_2O_2 and O_2^- accumulation compared with WT plants when subjected to MV treatment (Fig. 7). Increased UQ10 accumulation, acting as an antioxidant, may directly affect cellular antioxidation level (Ohara et al. 2004; Dutta et al. 2015), whereas the SOD and CAT enzymes, at least partially or indirectly, play a role in scavenging ROS in transgenic plants, indicating that non-enzymatic antioxidant UQ10 could cooperate with enzymatic antioxidants such as SOD and CAT to protect their cells from oxidative stress by scavenging ROS. Correspondingly, overexpression of 4-hydroxybenzoate prenyl diphosphate transferase (*SmPPT*) increased UQ accumulation and improved salt tolerance by increasing CAT and peroxidase activities and reducing MDA and H_2O_2 accumulation in *S. miltiorrhiza* (Liu et al. 2019a). In conclusion, overexpression of *VvPDS* could increase UQ accumulation and elevate plant tolerance to MV stress at least partially by promoting the SOD and CAT activities to scavenge ROS.

Conclusion

Based on phylogenetic analysis, subcellular localization, and both genetic complementation and biochemical assays, we reevaluated the role and function of VvPDS. Our results clearly established that VvPDS was an authentic *trans*-LC-PDS required for UQ10 biosynthesis, rather than a C_{10}-GDS enzyme involved in monoterpene biosynthesis as originally reported. A high level of UQ directly promotes oxidative stresses tolerance in plants by improving the radical scavenging ability. These findings not only provide insights for further evaluation of the enzyme activity and physiological functions of the long-chain PDSs but also enhance our understanding of terpene biosynthesis in grape.

Materials and methods

Plant material, hormone treatment and sample collection

N. benthamiana plants were cultured in a growth chamber at 25 °C in 16-h/8-h light/dark condition. The Chinese wild grapevine species *V. quinquangularis* accession "Danfeng-2" used for transient transformation was cultivated in the grape germplasm collection at Qingdao Agricultural University, Qingdao, China. Four popular table grape cultivars with different flavors, including "Fujiminori" (*V. vinifera* L. × *Vitis labrusca* L.), "Kyoho" (*V. vinifera* L. × *V. labrusca* L.), "Jumeigui" (*V. vinifera* L. × *V. labrusca* L.) and "Muscat Hamburg" (*V. vinifera* L.), were collected from own-rooted vines during August, 2023, Qingdao Agricultural University Pingdu Experimental Station (Qingdao, China, E119°91′, N36°98′). "Fujiminori" and "Kyoho" are traditional table grape cultivars without a muscat

flavor, while "Jumeigui" and "Muscat Hamburg" are known for their strong muscat flavor. All 4 grape cultivars were cultivated under the same climate and management conditions, including soil fertility, irrigation, training, and pruning. Ten healthy clusters (~300 grape berries) from 3 biological replicates were randomly harvested at 3 development stages, including EL34, EL36, and EL38, following the E-L system (Coombe 1995).

Furthermore, muscat grape cultivar "Muscat Hamburg" was used to investigate the association between *VvPDS* gene expression and monoterpene production in response to MeJA. The grape berries from 3 biological replicates at the EL34 stage were sprayed with 100 μM MeJA in deionized water with 0.05% (v/v) Tween-20 solution. Control (CK) groups were sprayed with deionized water containing 0.05% (v/v) Tween 20 solution. Grape samples were harvested 0, 1, 3, 5, and 10 d after MeJA treatments. Additionally, young leaves (10 d old), mature leaves (30 d old), flowers, developing seeds at veraison and berries at 4 developmental stages (EL31, EL34, EL36, and EL38) were collected from own-rooted "Muscat Hamburg" grape (*V. vinifera* L.). All the collected samples were immediately frozen in liquid nitrogen and stored at −80 °C for subsequent RNA extraction and metabolome analysis.

Extraction and identification of the monoterpene compounds

The extraction of monoterpene compounds from each sample followed the procedure described in our previous studies (Liu et al. 2022; Leng et al. 2023). In briefly, 100 g of grape berries were ground with 1 g of polyvinylpolypyrrolidone in liquid nitrogen and homogenized at 4 °C for 4 h. The mixture was then immediately centrifuged at 4 °C for 10 min to obtain a clear juice. Subsequently, 5 mL of the grape juice were mixed with 1 g of sodium chloride and 10 μL of 4-methyl-2-pentanol (1.0018 g/L) in a 20 mL vial (Agilent, 5188-2753 Santa Clara, California, USA) capped with a silicone septum (Agilent, 8010-0139). All samples underwent extraction with 3 biological replicates.

The monoterpene compounds were absorbed by using headspace solid-phase microextraction (HS-SPME) and then analyzed through an Agilent 7890B-5977A gas chromatograph-mass spectrometer (GC-MS) as our previous described (Sun et al. 2020). The sample vial was incubated at 40 °C for 30 min under agitation at 250 rpm, and then the preconditioned SPME fiber was inserted into the headspace of the vial to extract volatiles for 30 min at 40 °C under the same agitation conditions. Then, the SPME fiber was immediately inserted into the GC injection port at 250 °C for 8 min to desorb the volatiles. A 60 m × 0.25 mm HP-INNOWAX capillary column with a 0.25 μm film thickness (J&W Scientific, Folsom, CA, USA) was used to separate the volatile compounds under a 1 mL/min flow rate of helium (carrier gas). The temperature program was set as follows: 50 °C for 1 min, increase to 220 °C at 3 °C/min and hold at 220 °C for 5 min. The ion source was maintained at 250 °C with an MSD transfer line temperature of 250 °C. Mass scans were performed from m/z 30 to 350 with an ionization voltage of 70 eV.

The analysis of monoterpene compounds was based on the retention indices of reference standards and the NIST14 mass spectra database, respectively. The quantification of monoterpene compounds was performed by standard calibration curves. α-Terpineol, β-citronellol, β-myrcene, D-limonene, 4-terpineol, citral, geraniol, geranic acid, linalool, nerol, and terpinolene standards (Sigma-Aldrich) were dissolved in methanol and then diluted in distilled water containing 200 g/L glucose and 7 g/L tartaric acid to generate 15 concentration levels (Liu et al. 2022). When standards were unavailable, semi-quantification was carried out by matching compounds with the same functional group or similar numbers of carbon atoms. In addition, the monoterpene compounds in tobacco (*N. tabacum*) leaves were also detected by SPME-GC-MS under similar conditions.

RNA extraction and RT-qPCR analysis

Total RNA of grape berries was extracted by using the RNAprep Pure Plant kit (TIANGEN, Beijing, China) following the manufacturer's instructions. The cDNAs were synthesized from 1.5 μg total RNA by using the HiScript II One Step reverse transcription-PCR kit (Vazyme, Nanjing, China). RT-qPCR was conducted by using the SYBR Premix Ex Taq II Kit (TaKaRa, Japan) with the ABI StepOnePlus real-time PCR system (Applied Biosystems, CA, USA). All experiments were performed with 3 biological replicates, and *VvActin* (AB073011) was used as the internal control. The relative expression level was calculated using the $2^{-\Delta\Delta Ct}$ method (Livak and Schmittgen 2001). All primers are provided in Supplementary Table S4.

Sequence feature and phylogenetic analysis

Multiple sequence alignments were generated by using DNAMAN software (Lynnon-BioSoft, CA, USA), and phylogenetic trees were constructed by using MEGA7.0 software via the neighbor-joining method with 1,000 bootstrap replicates.

Isolation and subcellular localization analysis of *VvPDS*

The coding sequence (CDS) of *VvPDS* (https://www.grapegenomics.com) without a stop codon was amplified from "Muscat Hamburg" (*V. vinifera* L.) grape cDNAs and inserted into pRI-EGFP vector stored in our laboratory, which contains the CaMV 35S promoter and the C-terminal green fluorescence protein (GFP) (Chen et al. 2019). The VvPDS-GFP recombinant plasmid was then transfected into the *Agrobacterium tumefaciens* strain GV3101 and subsequently injected into leaf epidermal cells of *N. benthamiana* plants using the method previously described by Sparkes et al. (2006). Three days after injection, GFP fluorescence in *N. benthamiana* cells was observed using a laser scanning confocal microscope (Zeiss LSM 880NLO, Germany), and the mitochondria were visualized by using Mitotracker Red CMXRos. GFP fluorescence signals and chloroplast autofluorescence were detected at 500 to 535 and 650 to 750 nm after excitation at a laser wavelength of 488 nm, respectively. Mitotracker fluorescence was detected at 548 to 684 nm after excitation at 543 nm.

Stable and transient transformation of *VvPDS* in tobacco and grape leaves

The full-length CDS of *VvPDS* was cloned into the Gateway entry vector pDONR221 (Karimi et al. 2002) via BP reaction and then transferred into the binary overexpression vector pK7WG2.0 (Karimi et al. 2002) by site-specific LR reaction. Furthermore, a 459-bp cDNA fragment of *VvPDS* was amplified and cloned into the pK7GWIWG2(II) vector (Karimi et al. 2002) by LR reaction for gene silencing through RNA interference (RNAi) in vivo. All the recombinant plasmid was then introduced into the *A. tumefaciens* strain GV3101. Tobacco (*N. tabacum*) stable transformation was carried out through leaf disc transformation using the *A. tumefaciens* method, as previously described (Horsch et al. 1986). Transgenic plants were selected using kanamycin (100 mg/mL), and the regenerated transgenic shoots were transferred to soil and acclimatized in a temperature-controlled glasshouse. Seedlings from 3 independent T3 homozygous transgenic lines were used in further investigations.

Transient transformation was performed in the leaves of Chinese wild grapevine species *V. quinquangularis* accession "Danfeng-2" by using our previously established method (Liu et al. 2022). A 459 nucleotides sequence in CDS was amplified by PCR (Supplementary Table S4), introduced in pDONR221 vector and LR cloned in pK7GWiWG2(II) vector to obtain VvPDS RNAi construct, and VvPDS was silenced in grape leaves by an intron-containing hairpin RNA (ihpRNA) splicing (Huang et al. 2019). Recombinant *A. tumefacien* (OD_{600} = 1.0 to 1.2) containing VvPDS-OE and $VvPDS_{459}$-pK7GWIWG2-RNAi were suspended in the infiltration buffer, respectively. The empty vector was selected as the control. Six mature grape leaves, serving as 6 technical replications, were infiltrated with a bacterial solution in a vacuum dryer, and then the leaves were incubated and covered by wet gauze in the dark at 22 °C for 3 d. The transparent parts of the leaves that were immersed in the bacterial solution were divided into 3 biological replicates for further UQ analysis.

Enzymatic activity assay of VvPDS in vitro

For enzymatic assays, VvPDS was inserted into the pET32a (His-tag), stored in our laboratory, and the construct was transformed into *E. coli* BL21 cells (Weidi Biotech, Shanghai, China). Enzymatic activity assays were performed by using GC-MS as previously described (Wei et al. 2024). The enzyme activity reaction contained 10 μL desalted VvPDS-His protein solution, 66 mM IPP, 44 mM DMAPP, and ddH_2O up to 100 μL to determine the VvPDS activity in vitro. After incubation at 30 °C for 2 h, the mixture was hydrolyzed by using 1 unit of calf intestinal alkaline phosphatase and 1 unit of apyrase at 30 °C for overnight. The volatile products were adsorbed by HS-SPME overnight and subjected to GC-MS. The temperature program was set as follows: 50 °C for 1 min, increase to 120 °C at 5 °C/min, 200 °C at 8 °C/min and 250 °C at 12 °C/min for 7 min. The mass spectrometry (MS) conditions included the ionization energy of 70 eV, emission current of 200 mA, and a mass scan range of 29 to 600 amu.

Functional complementation of yeast *coq1* mutant

The full-length CDS of *VvPDS* was inserted into the yeast expression vector pRS426 (Morgan et al. 2019). *AtPDS* (At2g34630) and *OsGDS* (Os01g14630) were transferred into pRS426 to serve as positive and negative controls. These constructs, along with the empty vector pRS426, were separately transformed into the *S. cerevisiae coq1* mutant (strain Y13138), which was purchased from Euroscarf (http://www.euroscarf.de/index.php?name=News). Yeast cells were transformed using Yeast Transformation System 2 (TAKARA, Cat. Nos. 630439, Japan). Transformants were screened at 30 °C on SC-Ura plates (0.67% yeast nitrogen base with ammonium sulfate and a complete amino acid supplement lacking uracil) containing 2% glucose. A functional complementation assay was carried out as described previously (Ducluzeau et al. 2012; Xu et al. 2021). Yeast cells were plated on SC-Ura agar media containing 0.05% D-galactose as an inducer, along with either 2% glucose or 3% glycerol/2.5% ethanol as carbon sources. Plates were cultured at 30 °C for 2 d (glucose) or 7 d (glycerol/ethanol). Additionally, the WT yeast strain BY4741 and the yeast *coq1* mutant carrying the empty vector pRS426 were also employed as positive and negative controls, respectively.

UQ content analysis

Yeast cultivation and UQ extraction were performed as reported previously (Liu et al. 2019b) with some modifications. Yeast cells were cultured at 30 °C on YPD medium with 2% glucose as the carbon source until OD_{600} reached 1.2 to 1.6. Subsequently, 5 mL of the yeast cell suspension was centrifuged and washed twice with 2 mL water. After centrifugation, 1 mL of water containing 0.5 mL glass beads (0.5 mm) was added to the yeast pellet, and the mixture was vortexed for 10 min to disrupt the yeast cell wall. Samples were then extracted twice with 2 mL of 95% ethanol in an ultrasonic bath (50 Hz, 250 W). The supernatant was evaporated to dryness using gaseous nitrogen and resuspended in 0.5 mL spectroscopically pure ethanol. For grape and *N. tabacum* samples, 100 mg of freeze-dried samples were extracted with 5 mL of ethanol in an ultrasonic bath (50 Hz, 250 W) for 2 h. After centrifugation, the supernatant was evaporated to dryness with gaseous nitrogen and resuspended in 0.5 mL spectroscopically pure ethanol. Then, all supernatants were filtered through a C18 solid-phase extraction column (Agilent, USA) and a 0.22 μm membrane filter (Merk Millipore, USA) for LC-MS/MS analysis.

UQ was quantified by Agilent 1290 UPLC-6460 MS/MS system in MRM mode in positive ionization mode, including a triple quadrupole mass detector with an electrospray ionization source and an Agilent Poroshell 120 EC-C18 column (2.7 μm × 2.1 mm × 50 mm). The mobile phase used was ethanol and methanol in a 3:1 ratio with a flow rate of 0.2 mL/min under isocratic conditions. UQ6, UQ9 and UQ10 standards were purchased from Sigma-Aldrich and stored in darkness at −20 °C. Three independent biological replicates were carried out for each experimental condition.

Y2H, LUC assays, pull-down and co-IP

A Y2H assay was conducted by using the Matchmaker Gold Yeast Two-Hybrid System (Takara, Japan). The full-length CDS of *VvPDS* was cloned into the pGBKT7 or pGADT7 vectors, respectively. The resulting recombinant constructs were co-transformed into Y2H Gold cells using the LiCl-PEG method. The yeast cells were initially grown on SD/-Trp-Leu (-T/-L) plates and then transferred to SD/-Trp-Leu-His-Ade (-T/-L-H-A) plates for the screening of interactions.

For the LUC assay, *VvPDS* was respectively cloned into the pCAMBIA1300-nLUC (nLUC) and pCAMBIA1300-cLUC (cLUC) vectors, which were described previously in Chen et al. (2008). The *A. tumefaciens* strain GV3101 carrying VvPDS-nLUC and VvPDS-cLUC constructs were co-infiltrated into the leaves of 5 wk-old *N. benthamiana* plants as previous method (Wang et al. 2023a). Three days later, LUC images were captured using a CCD camera (Andor Technology, Belfast, UK).

To perform pull-down assay, *VvPDS* was respectively cloned into the pET32a (His-tag) and pGEX4T-1 (GST-tag) vectors, which were stored in our laboratory. VvPDS-His and GST/VvPDS-GST were expressed into *E. coli* BL21 cells (Weidi Biotech) use in a GST pull-down assay (Wang et al. 2023a). VvPDS-GST or the empty GST protein was immunoprecipitated using glutathione-sepharose beads (GeneScript, L00206) and incubated with VvPDS-His protein under gentle rotation (4 °C; 3 h). After 5 washes, 1 × SDS loading buffer was added into the bead-retained proteins, followed by boiling for 5 min. Subsequently, the samples were analyzed by 12% SDS-PAGE and visualized through Western blot assays using anti-GST (Beyotime Biotechnology, catalog number AF2888) and anti-HIS antibodies (Beyotime Biotechnology, catalog number AF2876).

For the co-IP assay, VvPDS was respectively cloned into the pRI-EGFP vector and pH7LIC4.1-FLAG vector. The *A. tumefaciens* strain GV3101 carrying VvPDS-GFP and VvPDS-FLAG were co-expressed in the leaves 5 wk-old *N. benthamiana* plants for 3 d. Total proteins were extracted using protein extraction buffer (50 mM Tris-MES, 0.5 M sucrose, 1 mM $MgCl_2$, 10 mM EDTA). The soluble proteins were incubated at 4 °C with 30 μL protein A/G magnetic

beads for 1 h followed by 50 μL anti-GFP antibody coupled magnetic beads (Chromo Tek) for 2 h as previously described (Hao et al. 2024). The precipitated proteins were washed 4 times with extraction buffer at 4 °C and then boiled in 1 × SDS loading buffer for analysis. The eluted proteins were separated immunoblotted with anti-FLAG (Sigma) and anti-GFP (Chromo Tek) antibodies.

MV treatment and oxidative stress analysis of tobacco plants

The 3-wk-old tobacco (*N. tabacum*) plants were sprayed with 50 μM MV (Sigma-Aldrich) in deionized water with 0.05% (v/v) Tween-20 solution. Then, these plants were kept for 3 d at 25 ± 1 °C under a day/night cycle of 16/8 h. Total chlorophyll (chlorophyll a + b) was extracted in 95% ethanol and quantified according to the previously described (Fitter et al. 2002). The MDA content was determined using thiobarbituric acid-based method (Ma et al. 2017). The accumulation of H_2O_2 and O_2^- in tobacco (*N. tabacum*) leaves were assessed through DAB and NBT histochemical staining, respectively. H_2O_2 content (H_2O_2-2-Y), O_2^- production rate (SA-2-G), SOD (SOD-2-Y), and CAT (CAT-2-Y) activities were measured following the manufacturer's instructions provided in the corresponding assay kits (Suzhou Keming Biotechnology Co., Ltd.). All experiment was conducted with 3 biological replicates.

Statistical analysis

All data were analyzed using the software SPSS 25.0. The data were represented as the means ± standard deviation (SD), and significant differences were compared using a 1-way ANOVA following Duncan's multiple range test at $P < 0.05$ level and independent *t*-tests, the results were noted by an asterisk (*$P < 0.05$, **$P < 0.01$).

Accession numbers

Sequence data from this article can be found in the GenBank/EMBL data libraries under accession numbers AmGDS.SSU, *Antirrhinum majus* GDS SSU (AAS82859); AmGDS.LSU, *A. majus* GDS LSU (AAS82860); MpGDS.SSU, *Mentha piperita* GDS SSU (AF182827); MpGDS.LSU, *M. piperita* GDS LSU (AF182828); HlGDS.SSU, *Humulus lupulus* GDS SSU (ACQ90681); HlGDS.LSU, *H. lupulus* GDS LSU (ACQ90682); CbGDS.SSU, *Clarkia breweri* GDS SSU (AAS82870); AtGGDS11, *Arabidopsis thaliana* GGDS11 (At4g36810); AtGGDS12, *A. thaliana* GGDS12 (At4g38460); CsGGDS.LSU, *Cucumis sativus* GGDS LSU (XP_031737098), CsGGDS.SSU1, *C. sativus* GGDS SSU 1 (XP_004139865); VvGGDS1, *Vitis vinifera* GGDS1 (VIT_04s0023g01210); VvGGDS2, *V. vinifera* GGDS2 (VIT_18s0001g12000); VvGGDS.SSU1, *V. vinifera* GGDS SSU 1 (VIT_19s0090g00530); VvGGDS.SSU2, *V. vinifera* GGDS SSU 2 (VIT_03s0038g03050); OsGDS, *Oryza sativa* GDS (Os01g14630); AgGDS1, *Abies grandis* GDS1 (AAN01133); AgGDS2, *A. grandis* GDS2 (AAN01134); AgGDS3, *A. grandis* GDS3 (AAN01135); CrGDS.LSU, *Catharanthus roseus* GDS LSU (JX417183); CrGDS.SSU, *C. roseus* GDS SSU (JX417184); CrSDS, *C. roseus* SDS (AHA82035); AaPDS, *Artemisia annua* PDS (PWA67664); PaGDS2, *Picea abies* GDS2 (ACA21458); PaSDS, *P. abies* SDS (ACA21459); VvPDS, *V. vinifera* PDS (VIT_15s0024g00850); VvSDS, *V. vinifera* SDS (VIT_19s0014g00070); AtPDS, *A. thaliana* PDS (AT2G34630); AtSDS1, *A. thaliana* SDS1 (AT1G78510); AtSDS2, *A. thaliana* SDS2 (AT1G17050); OsSDS1, *O. sativa* SDS1 (AK071299); OsSDS2, *O. sativa* SDS2 (AK066579); SlSDS, *Solanum lycopersicum* SDS (ABI63627); SlPDS, *S. lycopersicum* PDS (XP_025888065); HbSDS, *Hevea brasiliensis* SDS (DQ437520); SmSDS, *S. miltiorrhiza* SDS (MH924998); SmPDS, *S. miltiorrhiza* PDS (JX090100); ScCOQ1, *S. cerevisiae* COQ1 (AAA34686); SpDDS1, *Schizosaccharomyces* DDS1 (BAA12314).

Acknowledgments

We acknowledge Prof. JingJing Xu of Shanghai Chenshan Botanical Garden for the provision of yeast *coq1* mutant. We also thank to the support of Qingdao Agricultural University Analysis and Testing Center for UQ analysis.

Author contributions

X.P.L., L.S., and Y.F.Z. designed the experiments; P.P.W., T.T.R., R.Y.Y., Y.Z.C., and Y.X. performed the research; G.W., Y.T.L., X.L.J., Y.R.R., and K.K.Z. analyzed the data; P.P.W. and X.P.L. wrote the article. All authors read and approved the final version for publication.

Supplementary data

The following materials are available in the online version of this article.

Supplementary Figure S1. Structure-based multiple sequence alignment of *trans*-long-chain PDSs from various plant species. Seven domains conserved in eukaryotic polyprenyl diphosphate synthases were underlined and indicated by "I" to "VII." The conserved functional motifs, FARM and SARM signature were indicated by red box. M, mitochondria; C, chloroplast. The accession numbers were listed as follows: VvPDS (VIT_15s0024g00850), AtPDS (AT2G34630), CrSDS (AHA82035), OsSDS1 (AK071299), SmPDS (JX090100), AtSDS2 (AT1G17050), OsSDS2 (AK066579), SlSDS (ABI63627), and SmSDS (MH924998).

Supplementary Figure S2. Full-length amino acid sequence identity of VvPDS with *trans*-LC/SC-PDSs.

Supplementary Figure S3. Expression profiles of VvPDS and UQ biosynthesis-related genes in 54 grape organs during development (Fasoli et al. 2012). Transcriptomic data for gene expression analysis of Corvina atlas were retrieved from the NCBI GEO DataSets (GSE36128), which contained 54 various organs/tissues at different developmental stages. Data were normalized based on the mean expression value of each gene in all tissues. Red and green boxes indicate high and low expression levels, respectively, for each gene. Bud-AB, bud after burst; Bud-B, bud burst; Bud-L, latent bud; Bud-S, bud swell; Bud-W, winter bud; Flower-F, flowering; Flower-FB, flowering begins; FS, fruitset; Inflorescence-WD, well-developed; Inflorescence-Y, young; Leaf-FS, senescing leaf; Leaf-WD, mature; Leaf-Y, young; MR, mid-ripening; PFS, post-fruitset; R, ripening; Stem-G, green; Stem-W, woody; Tendril-FS, mature; Tendril-WD, well-developed; Tendril-Y, young; V, veraison.

Supplementary Figure S4. LC-MS/MS chromatograms showing the UQ products in different grape tissues. YL, young leaf; ML, mature leaf; F, flowers; B-EL31, berries pea-size; B-EL34, berries begin to soften; B-EL36, berries with intermediate Brix values; B-EL38, berries harvest-ripe; S, developing seeds at veraison.

Supplementary Figure S5. Monoterpene content and *NtSDS* expression in VvPDS transgenic and wild-type (WT) tobacco leaves. **A)** Limonene content; **B)** linalool content; **C)** total monoterpenes content in VvPDS transgenic and WT tobacco leaves; **D)** the expression level of *NtSDS* in tobacco leaves after stable overexpression of *VvPDS*. The values were presented as the means ± SD of 3 biological replicates, and the letters represent significant differences at $P < 0.05$.

Supplementary Figure S6. The formation of heteromeric complex between VvPDS and its homologous proteins in yeast 2-hybrid assays. BD-53 + AD-T7 and BD-Lam + AD-T7 were used as positive and negative controls, respectively.

Supplementary Table S1. The total monoterpene contents in 4 different grape cultivars during ripening.

Supplementary Table S2. The monoterpene contents in response to MeJA treatment in "Muscat Hamburg" grape.

Supplementary Table S3. Expression profiles of VvPDS and UQ biosynthesis-related genes in 54 grape organs during development.

Supplementary Table S4. All primers used in vector construction and qRT-PCR.

Funding

This research was supported by the National Natural Science Foundation of China (NSFC) (32372646, 32472677, 32002005, and 32002001), the BAAFS Funding for the Development of Distinguished Scientist (JKZX202402), the Key Research and Development Plan of Shandong Province (2024LZGC033, 2023TZXD015, and 2022TZXD001101) and Qingdao Natural Science Foundation (24-4-4-zrjj-135-jch), and Qingdao Agricultural University Enterprise Cooperation Projects (660/2425089).

Conflict of interest statement. None declared.

Data availability

Transcriptomic data for gene expression analysis of Corvina atlas were retrieved from the NCBI GEO DataSets (GSE36128).

References

Aharoni A, Jongsma MA, Bouwmeester HJ. Volatile science? Metabolic engineering of terpenoids in plants. *Trends Plant Sci*. 2005:10(12):594–602. https://doi.org/10.1016/j.tplants.2005.10.005

Ashby MN, Edwards PA. Elucidation of the deficiency in two yeast coenzyme Q mutants. Characterization of the structural gene encoding hexaprenyl pyrophosphate synthetase. *J Biol Chem*. 1990:265(22):13157–13164. https://doi.org/10.1016/S0021-9258(19)38280-8

Athanasakoglou A, Grypioti E, Michailidou S, Ignea C, Makris AM, Kalantidis K, Massé G, Argiriou A, Verret F, Kampranis SC. Isoprenoid biosynthesis in the diatom *Haslea ostrearia*. *New Phytol*. 2019:222(1):230–243. https://doi.org/10.1111/nph.15586

Block A, Fristedt R, Rogers S, Kumar J, Barnes B, Barnes J, Elowsky CG, Wamboldt Y, Mackenzie SA, Redding K, *et al.* Functional modeling identifies paralogous solanesyl-diphosphate synthases that assemble the side chain of plastoquinone-9 in plastids. *J Biol Chem*. 2013:288(38):27594–27606. https://doi.org/10.1074/jbc.M113.492769

Bosman RN, Lashbrooke JG. Grapevine mono- and sesquiterpenes: genetics, metabolism, and ecophysiology. *Front Plant Sci*. 2023:14:1111392. https://doi.org/10.3389/fpls.2023.1111392

Bouvier F, Suire C, d'Harlingue A, Backhaus RA, Camara B. Molecular cloning of geranyl diphosphate synthase and compartmentation of monoterpene synthesis in plant cells. *Plant J*. 2000:24(2):241–252. https://doi.org/10.1046/j.1365-313x.2000.00875.x

Burke CC, Croteau R. Geranyl diphosphate synthase from *Abies grandis*: cDNA isolation, functional expression, and characterization. *Arch Biochem Biophys*. 2002:405(1):130–136. https://doi.org/10.1016/S0003-9861(02)00335-1

Burke CC, Wildung MR, Croteau R. Geranyl diphosphate synthase: cloning, expression, and characterization of this prenyltransferase as a heterodimer. *Proc Natl Acad Sci U S A*. 1999:96(23):13062–13067. https://doi.org/10.1073/pnas.96.23.13062

Chen HM, Zou Y, Shang YL, Lin HQ, Wang YJ, Cai R, Tang XY, Zhou JM. Firefly luciferase complementation imaging assay for protein-protein interactions in plants. *Plant Physiol*. 2008:146(2):368–376. https://doi.org/10.1104/pp.107.111740

Chen KQ, Song MR, Guo YN, Liu LF, Xue H, Dai HY, Zhang ZH. MdMYB46 could enhance salt and osmotic stress tolerance in apple by directly activating stress-responsive signals. *Plant Biotechnol J*. 2019:17(12):2341–2355. https://doi.org/10.1111/pbi.13151

Chen QW, Fan DJ, Wang GD. Heteromeric geranyl(geranyl) diphosphate synthase is involved in monoterpene biosynthesis in Arabidopsis flowers. *Mol Plant*. 2015:8(9):1434–1437. https://doi.org/10.1016/j.molp.2015.05.001

Clastre M, Bantignies B, Feron G, Soler E, Ambid C. Purification and characterization of geranyl diphosphate synthase from *Vitis vinifera*. cv Muscat de Frontignan cell cultures. *Plant Physiol*. 1993:102(1):205–211. https://doi.org/10.1104/pp.102.1.205

Coombe BG. Growth stages of the grapevine: adoption of a system for identifying grapevine growth stages. *Aust J Grape Wine Res*. 1995:1(2):104–110. https://doi.org/10.1111/j.1755-0238.1995.tb00086.x

De Geyter N, Gholami A, Goormachtig S, Goossens A. Transcriptional machineries in jasmonate-elicited plant secondary metabolism. *Trends Plant Sci*. 2012:17(6):349–359. https://doi.org/10.1016/j.tplants.2012.03.001

Dong L, Jongedijk E, Bouwmeester H, Van Der Krol A. Monoterpene biosynthesis potential of plant subcellular compartments. *New Phytol*. 2016:209(2):679–690. https://doi.org/10.1111/nph.13629

D'Onofrio C, Matarese F, Cuzzola A. Effect of methyl jasmonate on the aroma of Sangiovese grapes and wines. *Food Chem*. 2018:242:352–361. https://doi.org/10.1016/j.foodchem.2017.09.084

Ducluzeau AL, Wamboldt Y, Elowsky CG, Mackenzie SA, Schuurink RC, Basset GJC. Gene network reconstruction identifies the authentic *trans*-prenyl diphosphate synthase that makes the solanesyl moiety of ubiquinone-9 in *Arabidopsis*. *Plant J*. 2012:69(2):366–375. https://doi.org/10.1111/j.1365-313X.2011.04796.x

Dutta A, Chan SH, Pauli NT, Raina R. HYPERSENSITIVE RESPONSE-LIKE LESIONS 1 codes for AtPPT1 and regulates accumulation of ROS and defense against bacterial pathogen *Pseudomonas syringae* in *Arabidopsis thaliana*. *Antioxid Redox Signal*. 2015:22(9):785–796. https://doi.org/10.1089/ars.2014.5963

Fan H, Liu Y, Li CY, Jiang Y, Song JJ, Yang L, Zhao Q, Hu YH, Chen XY, Xu JJ. Engineering high coenzyme Q10 tomato. *Metab Eng*. 2021:68:86–93. https://doi.org/10.1016/j.ymben.2021.09.007

Fasoli M, Dal Santo S, Zenoni S, Tornielli GB, Farina L, Zamboni A, Porceddu A, Venturini L, Bicego M, Vetal M. The grapevine expressionatlas reveals a deep transcriptome shift driving the entire plant into amaturation program. *Plant Cell*. 2012:24(9):3489–3505. https://doi.org/10.1105/tpc.112.100230

Feng YC, Morgan RML, Fraser PD, Hellgardt K, Nixon PJ. Crystal structure of geranylgeranyl pyrophosphate synthase (CrtE) involved in Cyanobacterial terpenoid biosynthesis. *Front Plant Sci*. 2020:11:589. https://doi.org/10.3389/fpls.2020.00589

Fitter DW, Martin DJ, Copley MJ, Scotland RW, Langdale JA. *GLK* gene pairs regulate chloroplast development in diverse plant species. *Plant J*. 2002:31(6):713–727. https://doi.org/10.1046/j.1365-313X.2002.01390.x

Gershenzon J, Dudareva N. The function of terpene natural products in the natural world. *Nat Chem Biol*. 2007:3(7):408–414. https://doi.org/10.1038/nchembio.2007.5

Guo RT, Kuo CJ, Chou CC, Ko TP, Shr HL, Liang PH, Wang AH. Crystal structure of octaprenyl pyrophosphate synthase from hyperthermophilic *Thermotoga maritima* and mechanism of product chain length determination. *J Biol Chem*. 2004:279(6):4903–4912. https://doi.org/10.1074/jbc.M310161200

Gutensohn M, Nagegowda DA, Dudareva N. Involvement of compartmentalization in monoterpene and sesquiterpene

biosynthesis in plants. In: Bach T, Rohmer M, editors. *Isoprenoid synthesis plants microorganisms*. New York (NY): Springer; 2013. p. 155–169.

Hao QX, Zhu XJ, Huang YS, Song JW, Mou CL, Zhang FL, Miao R, Ma TF, Wang P, Zhu ZY, *et al.* E3 ligase DECREASED GRAIN SIZE 1 promotes degradation of a G-protein subunit and positively regulates grain size in rice. *Plant Physiol*. 2024:196(2):948–960. https://doi.org/10.1093/plphys/kiae331

Horsch RB, Klee HJ, Stachel S, Winans SC, Nester EW, Rogers SG, Fraley RT. Analysis of *Agrobacterium tumefaciens* virulence mutants in leaf discs. *Proc Natl Acad Sci USA*. 1986:83(8):2571–2575. https://doi.org/10.1073/pnas.83.8.2571

Hsieh FL, Chang TH, Ko TP, Wang AHJ. Structure and mechanism of an Arabidopsis medium/long-chain-length prenyl pyrophosphate synthase. *Plant Physiol*. 2011:155(3):1079–1090. https://doi.org/10.1104/pp.110.168799

Huang Y, Xu PH, Hou BZ, Shen YY. Strawberry tonoplast transporter, FaVPT1, controls phosphate accumulation and fruit quality. *Plant Cell Environ*. 2019:42(9):2715–2729. https://doi.org/10.1111/pce.13598

Ji XH, Wang BL, Wang XD, Wang XL, Liu FZ, Wang HB. Differences of aroma development and metabolic pathway gene expression between Kyoho and 87-1 grapes. *J Integr Agric*. 2021:20(6):1525–1539. https://doi.org/10.1016/S2095-3119(20)63481-5

Jones MO, Perez-Fons L, Robertson FP, Bramley PM, Fraser PD. Functional characterization of long-chain prenyl diphosphate synthases from tomato. *Biochem J*. 2013:449(3):729–740. https://doi.org/10.1042/BJ20120988

Kainou T, Okada K, Suzuki K, Nakagawa T, Matsuda H, Kawamukai M. Dimer formation of octaprenyl-diphosphate synthase (IspB) is essential for chain length determination of ubiquinone. *J Biol Chem*. 2001:276(11):7876–7883. https://doi.org/10.1074/jbc.M007472200

Karimi M, Inzé D, Depicker A. GATEWAY™ vectors for *Agrobacterium*-mediated plant transformation. *Trends Plant Sci*. 2002:7(5):193–195. https://doi.org/10.1016/S1360-1385(02)02251-3

Kawamukai M. Biosynthesis and applications of prenylquinones. *Biosci Biotechnol Biochem*. 2018:82(6):963–977. https://doi.org/10.1080/09168451.2018.1433020

Kawamukai M. Biosynthesis and bioproduction of coenzyme Q_{10} by yeasts and other organisms. *Biotechnol Appl Biochem*. 2009:53(4):217–226. https://doi.org/10.1042/BA20090035

Kawamukai M. Biosynthesis, bioproduction and novel roles of ubiquinone. *J Biosci Bioeng*. 2002:94(6):511–517. https://doi.org/10.1016/S1389-1723(02)80188-8

Koksal M, Jin Y, Coates RM, Croteau R, Christianson DW. Taxadiene synthase structure and evolution of modular architecture in terpene biosynthesis. *Nature*. 2011:469(7328):116–120. https://doi.org/10.1038/nature09628

Leng XP, Cong JM, Cheng LX, Wan HL, Liu YX, Yuan YB, Fang JG. Identification of key gene networks controlling monoterpene biosynthesis during grape ripening by integrating transcriptome and metabolite profiling. *Hortic Plant J*. 2023:9(5):931–946. https://doi.org/10.1016/j.hpj.2023.03.005

Li W, Li WF, Yang SJ, Ma ZH, Zhou Q, Mao J, Han SY, Chen BH. Transcriptome and metabolite conjoint analysis reveals that exogenous methyl jasmonate regulates monoterpene synthesis in grape berry skin. *J Agric Food Chem*. 2020:68(18):5270–5281. https://doi.org/10.1021/acs.jafc.0c00476

Liu MM, Chen X, Wang MZ, Lu SF. SmPPT, a 4-hydroxybenzoate polyprenyl diphosphate transferase gene involved in ubiquinone biosynthesis, confers salt tolerance in *Salvia miltiorrhiza*. *Plant Cell Rep*. 2019a:38(12):1527–1540. https://doi.org/10.1007/s00299-019-02463-5

Liu MM, Lu SF. Plastoquinone and ubiquinone in plants: biosynthesis, physiological function and metabolic engineering. *Front Plant Sci*. 2016:7:1898. https://doi.org/10.3389/fpls.2016.01898

Liu MM, Ma YM, Du Q, Hou XM, Wang MZ, Lu SF. Functional analysis of polyprenyl diphosphate synthase genes involved in plastoquinone and ubiquinone biosynthesis in *Salvia miltiorrhiza*. *Front Plant Sci*. 2019b:10:893. https://doi.org/10.3389/fpls.2019.00893

Liu SY, Shan BQ, Zhou XM, Gao WP, Liu YR, Zhu BQ, Sun L. Transcriptome and metabolomics integrated analysis reveals terpene synthesis genes controlling linalool synthesis in grape berries. *J Agric Food Chem*. 2022:70(29):9084–9094. https://doi.org/10.1021/acs.jafc.2c00368

Livak KJ, Schmittgen TD. Analysis of relative gene expression data using realtime quantitative PCR and the $2^{-\Delta\Delta CT}$ method. *Methods*. 2001:25(4):402–408. https://doi.org/10.1006/meth.2001.1262

Ma QJ, Sun MH, Lu J, Liu YJ, You CX, Hao YJ. An apple CIPK protein kinase targets a novel residue of AREB transcription factor for ABA-dependent phosphorylation. *Plant Cell Environ*. 2017:40(10):2207–2219. https://doi.org/10.1111/pce.13013

Martin DM, Chiang A, Lund ST, Bohlmann J. Biosynthesis of wine aroma: transcript profiles of hydroxymethylbutenyl diphosphate reductase, geranyl diphosphate synthase, and linalool/nerolidol synthase parallel monoterpenol glycoside accumulation in Gewurztraminer grapes. *Planta*. 2012:236(3):919–929. https://doi.org/10.1007/s00425-012-1704-0

Mattila P, Kumpulainen J. Coenzymes Q9 and Q10: contents in foods and dietary intake. *J Food Compos Anal*. 2001:14(4):409–417. https://doi.org/10.1006/jfca.2000.0983

Morgan JT, Fink GR, Bartel DP. Excised linear introns regulate growth in yeast. *Nature*. 2019:565(7741):606–611. https://doi.org/10.1038/s41586-018-0828-1

Moses T, Pollier J, Thevelein JM, Goossens A. Bioengineering of plant (tri)terpenoids: from metabolic engineering of plants to synthetic biology *in vivo* and *in vitro*. *New Phytol*. 2013:200(1):27–43. https://doi.org/10.1111/nph.12325

Nagegowda DA. Plant volatile terpenoid metabolism: biosynthetic genes, transcriptional regulation and subcellular compartmentation. *FEBS Lett*. 2010:584(14):2965–2973. https://doi.org/10.1016/j.febslet.2010.05.045

Nagegowda DA, Gupta P. Advances in biosynthesis, regulation, and metabolic engineering of plant specialized terpenoids. *Plant Sci*. 2020:294:110457. https://doi.org/10.1016/j.plantsci.2020.110457

Nagel R, Berasategui A, Paetz C, Gershenzon J, Schmidt A. Overexpression of an isoprenyl diphosphate synthase in spruce leads to unexpected terpene diversion products that function in plant defense. *Plant Physiol*. 2014:164(2):555–569. https://doi.org/10.1104/pp.113.228940

Ohara K, Kokado Y, Yamamoto H, Sato F, Yazaki K. Engineering of ubiquinone biosynthesis using the yeast *coq2* gene confers oxidative stress tolerance in transgenic tobacco. *Plant J*. 2004:40(5):734–743. https://doi.org/10.1111/j.1365-313X.2004.02246.x

Ohara K, Sasaki K, Yazaki K. Two solanesyl diphosphate synthases with different subcellular localizations and their respective physiological roles in *Oryza sativa*. *J Exp Bot*. 2010:61(10):2683–2692. https://doi.org/10.1093/jxb/erq103

Orlova I, Nagegowda DA, Kish CM, Gutensohn M, Maeda H, Varbanova M, Fridman E, Yamaguchi S, Hanada A, Kamiya Y, *et al.* The small subunit of snapdragon geranyl diphosphate synthase modifies the chain length specificity of tobacco geranylgeranyl diphosphate synthase in planta. *Plant Cell*. 2009:21(12):4002–4017. https://doi.org/10.1105/tpc.109.071282

Paramasivan K, Mutturi S. Progress in terpene synthesis strategies through engineering of *Saccharomyces cerevisiae*. *Crit Rev Biotechnol*. 2017:37(8):974–989. https://doi.org/10.1080/07388551.2017.1299679

Parmar SS, Jaiwal A, Dhankher OP, Jaiwal PK. Coenzyme Q10 production in plants: current status and future prospects. *Crit Rev Biotechnol*. 2015:35(2):152–164. https://doi.org/10.3109/07388551.2013.823594

Pichersky E, Noel JP, Dudareva N. Biosynthesis of plant volatiles: nature's diversity and ingenuity. *Science*. 2006:311(5762):808–811. https://doi.org/10.1126/science.1118510

Rai A, Smita SS, Singh AK, Shanker K, Nagegowda DA. Heteromeric and homomeric geranyl diphosphate synthases from Catharanthus roseus and their role in monoterpene indole alkaloid biosynthesis. *Mol Plant*. 2013:6(5):1531–1549. https://doi.org/10.1093/mp/sst058

Rosenkranz M, Chen YY, Zhu PY, Vlot AC. Volatile terpenes–mediators of plant-to-plant communication. *Plant J*. 2021:108(3):617–631. https://doi.org/10.1111/tpj.15453

Saiki R, Nagata A, Uchida N, Kainou T, Matsuda H, Kawamukai M. Fission yeast decaprenyl diphosphate synthase consists of Dps1 and the newly characterized Dlp1 protein in a novel heterotetrameric structure. *Eur J Biochem*. 2003:270(20):4113–4121. https://doi.org/10.1046/j.1432-1033.2003.03804.x

Schmidt A, Gershenzon J. Cloning and characterization of two different types of geranyl diphosphate synthases from Norway spruce (*Picea abies*). *Phytochemistry*. 2008:69(1):49–57. https://doi.org/10.1016/j.phytochem.2007.06.022

Shi XY, Cao S, Wang X, Huang SY, Wang Y, Liu ZJ, Liu WW, Leng XP, Peng YL, Wang N, *et al*. The complete reference genome for grapevine (*Vitis vinifera* L.) genetics and breeding. *Hortic Res*. 2023:10(5):uhad061. https://doi.org/10.1093/hr/uhad061

Sparkes IA, Runions J, Kearns A, Hawes C. Rapid, transient expression of fluorescent fusion proteins in tobacco plants and generation of stably transformed plants. *Nat Protoc*. 2006:1(4):2019–2025. https://doi.org/10.1038/nprot.2006.286

Sun L, Zhu BQ, Sun XR, Xu XQ, Zhang GJ, Yan AL, Xu HY. Monoterpene accumulation and its biosynthesis: gene transcript profiles of two grape cultivars during berry development. *Acta Hortic*. 2015:1082(1082):37–42. https://doi.org/10.17660/ActaHortic.2015.1082.2

Sun L, Zhu BQ, Zhang XY, Wang HL, Yan AL, Zhang GJ, Wang XY, Xu HY. The accumulation profiles of terpene metabolites in three Muscat table grape cultivars through HS-SPME-GCMS. *Sci Data*. 2020:7(1):5. https://doi.org/10.1038/s41597-019-0321-1

Swiezewska E. Ubiquinone and plastoquinone metabolism in plants. *Methods Enzymol*. 2004:378:124–131. https://doi.org/10.1016/S0076-6879(04)78007-6

Teixeira A, Martins V, Frusciante S, Cruz T, Noronha H, Diretto G, Gerós H. Flavescence doree-derived leaf yellowing in grapevine (*Vitis vinifera* L.) is associated to a general repression of isoprenoid biosynthetic pathways. *Front Plant Sci*. 2020:11:896. https://doi.org/10.3389/fpls.2020.00896

Teixeira A, Noronha H, Frusciante S, Diretto G, Geros H. Biosynthesis of chlorophyll and other isoprenoids in the plastid of red grape berry skins. *J Agric Food Chem*. 2023:71(4):1873–1885. https://doi.org/10.1021/acs.jafc.2c07207

Tetali SD. Terpenes and isoprenoids: a wealth of compounds for global use. *Planta*. 2019:249(1):1–8. https://doi.org/10.1007/s00425-018-3056-x

Tholl D, Kish CM, Orlova I, Sherman D, Gershenzon J, Pichersky E, Dudareva N. Formation of monoterpenes in *Antirrhinum majus* and *Clarkia breweri* flowers involves heterodimeric geranyl diphosphate synthases. *Plant Cell*. 2004:16(4):977–992. https://doi.org/10.1105/tpc.020156

Tholl D, Lee S. Terpene specialized metabolism in *Arabidopsis thaliana*. *Arabidopsis Book*. 2011:9:e0143. https://doi.org/10.1199/tab.0143

van Schie CCN, Ament K, Schmidt A, Lange T, Haring MA, Schuurink RC. Geranyl diphosphate synthase is required for biosynthesis of gibberellins. *Plant J*. 2007:52(4):752–762. https://doi.org/10.1111/j.1365-313X.2007.03273.x

Vandermoten S, Haubruge E, Cusson M. New insights into short-chain prenyltransferases: structural features, evolutionary history and potential for selective inhibition. *Cell Mol Life Sci*. 2009:66(23):3685–3695. https://doi.org/10.1007/s00018-009-0100-9

Vranová E, Coman D, Gruissem W. Structure and dynamics of the isoprenoid pathway network. *Mol Plant*. 2012:5(2):318–333. https://doi.org/10.1093/mp/sss015

Vranová E, Coman D, Gruissem W. Network analysis of the MVA and MEP pathways for isoprenoid synthesis. *Annu Rev Plant Biol*. 2013:64(1):665–700. https://doi.org/10.1146/annurev-arplant-050312-120116

Wang CY, Chen QW, Fan DJ, Li JX, Wang GD, Zhang P. Structural analyses of short-chain prenyltransferases identify an evolutionarily conserved GFPPS clade in Brassicaceae plants. *Mol Plant*. 2016:9(2):195–204. https://doi.org/10.1016/j.molp.2015.10.010

Wang G, Dixon RA. Heterodimeric geranyl(geranyl) diphosphate synthase from hop (*Humulus lupulus*) and the evolution of monoterpene biosynthesis. *Proc Natl Acad Sci U S A*. 2009:106(24):9914–9919. https://doi.org/10.1073/pnas.0904069106

Wang K, Ohnuma S. Chain-length determination mechanism of isoprenyl diphosphate synthases and implications for molecular evolution. *Trends Biochem Sci*. 1999:24(11):445–451. https://doi.org/10.1016/S0968-0004(99)01464-4

Wang L, Wang YJ. Transcription factor *VqERF114* regulates stilbene synthesis in Chinese wild *Vitis quinquangularis* by interacting with VqMYB35. *Plant Cell Rep*. 2019:38(10):1347–1360. https://doi.org/10.1007/s00299-019-02456-4

Wang NN, Shi YY, Jiang Q, Li H, Fan WX, Feng Y, Li L, Liu B, Lin F, Jing W, *et al*. A 14-3-3 protein positively regulates rice salt tolerance by stabilizing phospholipase C1. *Plant Cell Environ*. 2023a:46(4):1232–1248. https://doi.org/10.1111/pce.14520

Wang W, Feng J, Wei LL, Khalil-Ur-Rehman M, Nieuwenhuizen NJ, Yang LN, Zheng H, Tao JM. Transcriptomics integrated with free and bound terpenoid aroma profiling during "Shine Muscat" (*Vitis labrusca* × *V. vinifera*) grape berry development reveals coordinate regulation of MEP pathway and terpene synthase gene expression. *J Agric Food Chem*. 2021:69(4):1413–1429. https://doi.org/10.1021/acs.jafc.0c06591

Wang W, Wang MY, Zeng YL, Chen XY, Wang XY, Barrington AM, Tao JM, Atkinson RG, Nieuwenhuizen NJ. The terpene synthase (TPS) gene family in kiwifruit shows high functional redundancy and a subset of TPS likely fulfil overlapping functions in fruit flavour, floral bouquet and defence. *Mol Hortic*. 2023b:3(1):9. https://doi.org/10.1186/s43897-023-00057-0

Wang Y, Hekimi S. Understanding ubiquinone. *Trends Cell Biol*. 2016:26(5):367–378. https://doi.org/10.1016/j.tcb.2015.12.007

Wei G, Chen YD, Wang JW, Feng LG. Molecular cloning and characterization of farnesyl diphosphate synthase from *Rosa rugosa* Thunb associated with salinity stress. *PeerJ*. 2024:12:e16929. https://doi.org/10.7717/peerj.16929

Wei G, Tian P, Zhang FX, Qin H, Miao H, Chen QW, Hu ZY, Li C, Wang MJ, Gu XF, *et al*. Integrative analyses of nontargeted volatile profiling and transcriptome data provide molecular insight into VOC diversity in cucumber plants (*Cucumis sativus*). *Plant Physiol*. 2016:172(1):603–618. https://doi.org/10.1104/pp.16.01051

Wei Y, Meng N, Wang YC, Cheng J, Duan CQ, Pan QH. Transcription factor VvWRKY70 inhibits both norisoprenoid and flavonol biosynthesis in grape. *Plant Physiol*. 2023:193(3):2055–2070. https://doi.org/10.1093/plphys/kiad423

Wen YQ, Zhong GY, Gao Y, Lan YB, Duan CQ, Pan QH. Using the combined analysis of transcripts and metabolites to propose key genes for differential terpene accumulation across two regions. *BMC Plant Biol*. 2015:15(1):240. https://doi.org/10.1186/s12870-015-0631-1

Xie S, Wu G, Ren RH, Xie R, Yin HN, Chen HW, Yang BW, Zhang ZW, Ge MS. Transcriptomic and metabolic analyses reveal differences in monoterpene profiles and the underlying molecular mechanisms in six grape varieties with different flavors. *LWT Food Sci Technol*. 2023:174:114442. https://doi.org/10.1016/j.lwt.2023.114442

Xu JJ, Zhang XF, Jiang Y, Fan H, Li JX, Li CY, Zhao Q, Yang L, Hu YH, Martin C, *et al*. A unique flavoenzyme operates in ubiquinone biosynthesis in photosynthesis-related eukaryotes. *Sci Adv*. 2021:7(50):eabl3594. https://doi.org/10.1126/sciadv.abl3594

Yin JL, Wong WS, Jang IC, Chua NH. Co-expression of peppermint geranyl diphosphate synthase small subunit enhances monoterpene production in transgenic tobacco plants. *New Phytol*. 2017:213(3):1133–1144. https://doi.org/10.1111/nph.14280

Yue XF, Ju YL, Fang YL, Zhang ZW. Transcriptomics integrated with metabolomics reveals the effect of cluster thinning on monoterpene biosynthesis in 'Muscat Hamburg' grape. *Foods*. 2021a:10(11):2718. https://doi.org/10.3390/foods10112718

Yue XF, Ju YL, Zhang HJ, Wang ZH, Xu HD, Zhang ZW. Integrated transcriptomic and metabolomic analysis reveals the changes in monoterpene compounds during the development of Muscat Hamburg (*Vitis vinifera* L.) grape berries. *Food Res Int*. 2022:162:112065. https://doi.org/10.1016/j.foodres.2022.112065

Yue XF, Liu SQ, Wei SC, Fang YL, Zhang ZW, Ju YL. Transcriptomic and metabolic analyses provide new insights into the effects of exogenous sucrose on monoterpene synthesis in "Muscat Hamburg" grapes. *J Agric Food Chem*. 2021b:69(14):4164–4176. https://doi.org/10.1021/acs.jafc.1c00420

Yue XF, Wei SC, Liu WH, Lu JS, Fang YL, Zhang ZW, Ju YL. Effect of rain-shelter cultivation on the monoterpenes profile of Muscat Hamburg grapes and wines. *Sci Hortic*. 2021c:285:110136. https://doi.org/10.1016/j.scienta.2021.110136

Zhang J, Ma YH, Chen QW, Yang MX, Feng DY, Zhou F, Wang GD, Wang CY. Functional prediction of *trans*-prenyltransferases reveals the distribution of GFPPSs in species beyond the Brassicaceae clade. *Int J Mol Sci*. 2022:23(16):9471. https://doi.org/10.3390/ijms23169471

Zhou F, Wang CY, Gutensohn M, Jiang L, Zhang P, Zhang DB, Dudareva N, Lu S. A recruiting protein of geranylgeranyl diphosphate synthase controls metabolic flux toward chlorophyll biosynthesis in rice. *Proc Natl Acad Sci U S A*. 2017:114(26):6866–6871. https://doi.org/10.1073/pnas.1705689114

Zhou SM, Liu SY, Gao WP, Hu BF, Zhu BQ, Sun L. Monoterpenoids evolution and MEP pathway gene expression profiles in seven table grape varieties. *Plants*. 2022:11(16):2143. https://doi.org/10.3390/plants11162143